NTNU

Norwegian University of
Science and Technology

Release and Spreading of Dense Gases

Turbulence modeling with Kameleon FireEx

Tarjei Bærland

Master of Science in Product Design and Manufacturing

Submission date: June 2011

Supervisor: Ivar Ståle Ertesvåg, EPT

Norwegian University of Science and Technology
Department of Energy and Process Engineering

Norges teknisk-
naturvitenskapelige universitet
NTNU

Fakultet for ingeniørvitenskap og teknologi
Institutt for energi- og prosessteknikk

NTNU

EPT-M-2011-63

MASTEROPPGAVE

for
Tarjei Bærland

Våren 2011

Utslipp og spredning av tung gass

Release and spreading of dense gases

Bakgrunn og formål

Ved NTNUs Institutt for energi- og prosessteknikk har det i en årrekke vært arbeidet med matematisk modellering og numerisk simulering av turbulent strømning og forbrenning. Metodene og modellene som er utviklet gjennom denne forskningsaktiviteten, har blitt anvendt på en rekke industrielle problemstillinger.

For å kunne beregne spredning av utslipp så realistisk og nøyaktig som mulig er det nødvendig med detaljert kunnskap om de fysiske og kjemiske prosessene som opptrer. Videre må en ha gode modeller for disse prosessene og for sammenhengen mellom dem.

I forbindelse med instituttets og ComputIT AS sitt engasjement innenfor sikkerhetsrelatert strømings- og forbrenningsteknikk, ønsker vi gjennom dette prosjektet å studere matematiske modeller for de ulike fysiske og kjemiske fenomenene som opptrer ved utslipp av tunge gasser i luft. Både brennbare (HC), giftige (t.d. H_2S) og kvelende (t.d. CO_2) gasser er av interesse.

Masteroppgaven er en videreføring av prosjektoppgaven fra høsten 2010 med samme tema.

Oppgaven bearbeides ut fra følgende punkter:

- Videre litteraturstudium over turbulent strømning og spredning av stoff i grensesjikt. I den grad det er relevant også supplere andre deler av litteraturstudiet utført i prosjektoppgaven.
- Vurdere numerisk vertøy (program) for å beregne spredning av tunge gasser. Sette seg inn i og presentere det valgte programet.
- Gjennomføre beregninger av spredning av tunge gasser basert på eksisterende modeller. Vurdere og prøve ut nye/modifiserte modeller. Diskutere resultatene.
- Diskutere eventuelle forbedringer av de matematiske modellene for spredning og utblanding av tung gass i luft.

En fremdriftsplan *(Planlagte aktiviteter med tidsplan for fremdrift)* for hele oppgaven skal forelegges faglærer/veileder(e) for kommentarer innen 14 dager etter utlevering av oppgaveteksten.

Besvarelsen redigeres mest mulig som en forskningsrapport med innholdsfortegnelse, et sammendrag på norsk, konklusjon, litteraturliste, etc. Ved utarbeidelsen av teksten skal kandidaten legge vekt på å gjøre teksten oversiktlig og velskrevet. Med henblikk på lesing av besvarelsen er det viktig at de nødvendige henvisninger for korresponderende steder i tekst, tabeller og figurer anføres på begge steder. Ved bedømmelsen legges det stor vekt på at resultatene er grundig bearbeidet, og at de oppstilles tabellarisk og/eller grafisk på en oversiktlig måte og diskuteres utførlig.

Det forutsettes at kandidaten på eget initiativ etablerer et tilfredsstillende kontaktforhold med faglærer og veileder(e).

Kandidaten skal rette seg etter arbeidsreglement ved ComputIT AS, samt etter eventuelt andre pålegg fra den ansvarlige ledelse. Det tillates ikke at kandidaten griper inn i betjeningen av anlegg, installasjoner og lignende uten etter avtale med ansvarshavende.

I henhold til "Utfyllende regler til studieforskriften for teknologistudiet/sivilingeniørstudiet" ved NTNU § 20, forbeholder instituttet seg retten til å benytte alle resultater i undervisnings- og forskningsformål, samt til publikasjoner.

Sluttrapport for oppgaven skal leveres innbundet i 3 komplette eksemplarer med et "løsblad" med konsentrert sammendrag med forfatternavn og oppgavetittel for eventuell referering i tidsskrifter (maksimalt én maskinskrevet side med dobbel linjeavstand. Ytterligere kopier av rapporten til evt. medveileder(e)/kontaktpersoner skal avtales med, og evt. leveres direkte til, de respektive. Til faglærer/instituttet innleveres også en komplett kopi på CD-ROM i Word-format eller tilsvarende.

Sluttrapporten skal innleveres til Instituttet *innen XX. juni 2011.*

Institutt for energi- og prosessteknikk, 17. januar 2010

Olav Bolland
Instituttleder

Ivar S. Ertesvåg
Faglærer/veileder

Medveiledere/kontaktpersoner:
Kjell Erik Rian, ComputIT AS
Nils Inge Lilleheie, ComputIT AS

Preface

This thesis is the culmination of five years of more or less intensive study. I have followed the master's program in Mechanical Engineering at NTNU, and been studying under the department of Energy and Process Engineering. The topic of this work was determined by the department in cooperation with Computational Industry Technologies AS.

It has been an interesting experience to work on this thesis. The editing in these final weeks saw to the removal of paragraphs written right after some long-forgotten artifact in the Kameleon FireEx code had been discovered—the internals of a computer program sure are messy. On that note, many thanks to Nils Inge Lilleheie, who has guided me through the process. For helping me with the use of KFX and gathering data, thank you, Kjell Erik and Rune. I have enjoyed my time at ComputIT and I am glad that everyone here has seen to that this year has not been all work.

I would also like to thank my supervisor, Ivar Ståle Ertesvåg for helping me understand how and why the models are as they are.

This thesis would not end up as it is if it were not for Mia and Øystein, meant in the best way possible. Finally, I want to thank Mette for having patience with me when the work on the thesis has been at its most engaging ... or frustrating.

Trondheim, June 2011

Tarjei Bærland

Abstract

A dense gas released into the atmosphere will have a flow development that can be described by a large range of physical scales and quantities. An instantaneous release will slump towards the ground unaffcted by the wind, before it is gradually and increasingly diluted by the turbulence in the surrounding flow. Therefore, when the gas is far from the release point, its movement is determined by that of the wind.

The wind's turbulence characteristics varies with the atmospheric stability. An unstably stratified boundary layer will have turbulence production by negative density gradients, regardless of free stream velocity. A stable stratification, however, requires a wind velocity and shear to produce turbulence. The wind profile's velocity and turbulence characteristics can be described by similarity models, which may further be used as initial and boundary conditions in a turbulence model.

The k-ε model is a second order turbulence closure that has proved succesful in describing several turbulent flow scenarios. The version of the model used in the software package Kameleon FireEx has here been tested for dense gas releases, with a focus on far field development. Wind modeling is an area where the standard k-ε model is known to have problems, as it gives an unrealistic, inhomogoneous flow field.

Three alterations to the k-ε model were tested in the work on this thesis. The first was a model constant varying with the local turbulence parameters, the second was a modification to the turbulence Schmidt number and, finally, a correctional production was added to the transport equations for k and ε. Of the three approaches, the last one gave the most encouraging results.

There are still problems left regarding the k-ε model's handling of buoyancy-affected diffusivity. The Schmidt number modification dampens the dense gas' ability to diffuse also in the lateral directions, not only in the vertical, an effect that should be investigated further.

Sammendrag

Et tungt gass-utslipp i atmosfæriske omgivelser vil ha en strømningsutvikling som kan beskrives ved hjelp av en mengde fysiske størrelser. Et momentant utslipp vil falle raskt mot bakken, ubemerket av vinden. Etter som den gradvis og økende blir tynnet ut av turbulensen i luften, vil gassens bevegelse bestemmes mer og mer av det atmosfæriske grensesjiktet.

Vindens turbulenskarakteristikker varierer med den atmosæriske stabiliteten. I et ustabilt grensesjikt vil det være turbulensproduksjon fra negative tetthetsgradienter, uavhengig av vindens fristrømshastighet. En stabil sjikting vil derimot behøve en vindhastighet og skjærspenninger for å produsere turbulens. Vindprofilets hastighets- og turbulensegenskaper kan beskrives med similaritetsmodeller, som igjen kan benyttes til initial- og grensebetingelser i en turbulensmodell.

k-ε-modellen er en annen ordens turbulensmodell som gjennom årene har vist at den kan beskrive flere typer turbulent strømning. Den versjonen av modellen som er implementert i CFD-programmet Kameleon FireEx blir her testet for tung gassspredning, med fokus på utviklingen av vindfeltet. Vindmodellering er et område hvor standardutgaven av k-ε-modellen har vist seg å ha problemer, og den leverer et urealistisk, inhomogent strømningsfelt.

Tre utbedringstilnærminger har blitt testet i arbeidet med denne avhandlingen. Den første var en modellkonstant som varierte med de lokale turbulensforholdene, den andre var en modeifikasjon av Schmidt-tallet og den siste var en korreksjonsproduksjon som ble lagt til transportligningene for k og ε. Av de tre tilnærmingene, ga kun den siste lovende resultater.

Det gjenstår fortsatt problemer ved k-ε-modellens håndtering av oppdriftspåvirket diffusivitet. Modifikasjonen av Schmidt-tallet dempet også gassens evne til å diffundere i lengderetningene, mens den ideelt sett kun skulle påvirke diffusjon i høyden. Denne effekten bør undersøkes nærmere.

Contents

Nomenclature

Roman Symbols

c_p	Specific heat under constant pressure	($\mathrm{Jkg^{-1}K^{-1}}$)
D	Diameter of cylinder	(m)
f	Coriois parameter	($\mathrm{s^{-1}}$)
g	Gravitational acceleration	($\mathrm{ms^{-2}}$)
g'	Reduced gravitational acceleration	($\mathrm{ms^{-2}}$)
H	Sensible heat flux at surface	($\mathrm{Wm^{-2}}$)
h	Gas cloud height	(m)
H_L	Ground heat flux to sub-surface medium	($\mathrm{Wm^{-2}}$)
H_L	Latent heat flux at surface	($\mathrm{Wm^{-2}}$)
k	Mean turbulence energy	($\mathrm{m^2s^{-2}}$)
z_0	Roughness scaling height	(m)
R_N	Net heat flux at surface	($\mathrm{Wm^{-2}}$)
L	Monin-Obhukov length scale	(m)
Re_D	Reynolds number	
Ri_0	Initial Richardson number	
Ri_f	Flux Richardson number	
Ri_*	Richardson number based on wind's shear velocity	
U	Characteristic velocity	($\mathrm{ms^{-1}}$)
u	Flow velocity	($\mathrm{ms^{-1}}$)
u_*	Surface shear velocity	($\mathrm{ms^{-1}}$)
w_e	Vertical entrainment velocity	($\mathrm{ms^{-1}}$)

x_i	Cartesian coordinate i	

Greek Symbols

α	Volumetric coefficient of expansion	(K^{-1})
$\Gamma_{\phi,\text{eff}}$	Effective diffusion coefficient for flow variable ϕ	
γ	Dry adiabatic lapse rate	(Km^{-1})
δ_{ij}	Kronecker delta	
ε	Mean dissipation rate of turbulence energy	(m^2s^{-3})
ζ	Atmospheric stability parameter, $\zeta = z/L$	
θ	Temperature	(K)
ϑ	Difference between local and adiabatic temperature	(K)
κ	von Karman's constant and wavenumber	(–,m^{-1})
Λ	Local scaling parameter for atmospheric boundary layers	(m)
λ	Molecular conductivity	($Jm^{-1}s^{-1}K^{-1}$)
μ	Molecular dynamic viscosity	(kg $m^{-1}s^{-1}$)
μ_t	Turbulence related dynamic viscosity	(kg $m^{-1}s^{-1}$)
ν	Molecular kinematic viscosity	(m^2s^{-1})
ν_t	Turbulence related kinematicviscosity	(m^2s^{-1})
ρ	Gas density	(kgm^{-3})
ρ_a	Density of air	(kgm^{-3})
ρ_r	Relative density	
σ_ϕ	Molecular Prandtl-Schmidt number for flow variable ϕ	
$\sigma_{\phi t}$	Turbulence Prandtl-Schmidt number for flow variable ϕ	
Ω	Rotational speed of the Earth	(s^{-1})

Sub- and superscripts

$'$	Fluctuating value, Reynolds decomposition (or reduced quantity)
$''$	Fluctuating value, Favre decomposition
$\bar{}$	Reynolds average
$\tilde{}$	Favre average

0	Initial value, also used for surface value (τ)
a	Atmospheric property
ad	Adiabatic

Abbreviations and Dimensionless Numbers

CFD	Computational fluid dynamics
DNS	Direct numerical simulation
LES	Large eddy simulation
LFL	Lower flammability limit
LNG	Liquefied natural gas
MP	Measuring point
PBL	Atmospheric planetary boundary layer
PDE	Partial differential equations
ppm	Parts per million
RANS	Reynolds-averaged Navier-Stokes
RPT	Rapid phase transition
SIMPLEC	Semi-Implicit Method for Pressure-Linked Equations Consistent
SOU	Second order upwind numerical scheme
SWE	Shallow water equation
UFL	Upper flammability limit

1 Introduction

The dispersion of dense gases is of increasing interest in the process industry. A dense gas' momentum will be driven by negative buoyancy, which spreads the gas along the ground, thereby posing an added threat of exposure at the surface. As computers get more powerful, if not more sophisticated, they are used to model releases over larger and larger scales. When both the scales and the expectations for accuracy grow, there will be a higher demand on the modeling of the wind field, dilution processes and geometry interaction.

The topic of this thesis is dense gas dispersion in an atmospheric boundary layer, with a focus on large scale releases.

1.1 A continuation of previous work

This master's thesis is a continuation of a specialization project that was finished in the fall of 2010 (Bærland, 2010). The topic of the project was dense gas dispersion and experimental data was compared with simulation results obtained through the computer program Kameleon FireEx. To ensure that this thesis can be read separately, some of the results and comments from the project report are repeated here.

The most prominent feature of the results in the specialization project was the fast dispersion of dense gas over an impenetrable object. Gas was transported over a fence quicker in the simulation than the experimental data indicated. Intuitively, there seems to be a few explanations for this. The diluting effect of the wind may be overestimated, or the wind might have a too large convective effect along the ground.

The aim of this thesis is to find any shortcomings of the dense gas modeling in the commercial CFD packages Kameleon FireEx. Alterations to the models are then suggested and assessed. Since the focus is somewhat shifted from that of the project, towards larger scale effects, there is done a literature of atmospheric boundary layers.

To better isolate the dense gas effects, the gases considered in this work are arbitrary, isotherm gases—as were also the case in the project. The exception is Sec. 2.3, where specific hazardous effects are outlined.

1.2 Structure of the thesis

The next chapter treats the general aspects of a dense gas release. One conclusion here is that gas dispersion is greatly controlled by the surrounding wind, making

the modeling of the wind field a key component regarding a dense gas release. The third chapter is therefore devoted to the atmospheric boundary layer, its layer wise distribution and a central similarity model for this, the theory of Monin and Obukhov. This finishes the descriptive part of the physics, and the next chapters introduce the k-ε turbulence model and how this is implemented numerically in KFX.

The current version of KFX is then tested to a higher degree than that in the previous work, and trouble areas are located. In the final chapter, a number of alterations are suggested, tested and assessed.

2 Dense gas

At standard atmospheric conditions,[1] the air around us has a density of approximately 1.2 kg/m^3. What is known as a dense, or "heavy", gas is a gas that is denser than this air, a denser-than-air gas. Flows of these gases in an otherwise standard atmosphere show some interesting phenomena.

This chapter acts as an introduction to dense gases. Their characteristics are outlined, as are the different flow phenomena that occur in a dense gas release. The main reason for the interest in dense gases, namely that they are often hazardous, are emphasized towards the end of the chapter.

2.1 Characteristics of a dense gas

In this section, some characteristics of dense gases and the flow of these are described. These characteristics apply to an arbitrary dense gas.

2.1.1 Dimensionless numbers

Dimensionless numbers are, if not exclusively, used to generalize physical relations and comparing the contributions of different terms in equations. A typical form of a dimensionless number is a fraction that compares the effect of one physical quantity to another's. Some dimensionless numbers are especially relevant when studying dense gas flow.

As is evident, the density difference between the two fluids (i.e. the dense gas and the surrounding air) is important. The gravity the denser gas feels relative to the air's is expressed by the reduced gravitational accelerations,

$$g' = g\frac{\rho - \rho_a}{\rho_a}, \tag{2.1}$$

where ρ is the density of the dense gas and ρ_a is that of the surrounding air. g is the regular gravitational acceleration.

While the dimensional quantity g' expresses the effect of the density difference in a still environment, the influence of this compared to that of the advectional effect of the wind's movement is quantified by the initial Richardson number,

$$\mathrm{Ri}_0 = \frac{g'_0 h_0}{U_0^2}, \tag{2.2}$$

[1] By the ISO 5011 standard, atmospheric conditions are a temperature of 20 °C and pressure of 101.3 kPa.

where h is the cloud's height and U is a characteristic velocity of the surrounding wind. The subscript 0 denotes initial values, which indicates that Ri_0 describes the flow "out of the gate". For releases with $\mathrm{Ri}_0 \approx 1$, both the gravitational force and the drag force contribute noticeably to the fluid motion (Rottman *et al.*, 1985*a*).

Britter & McQuaid (1988) propose their own dimensionless groups for categorizing whether a dispersion process is "passive" (i.e. behaves as a neutrally buoyant release) or whether the buoyancy effects should be accounted for. Such categorizations are most valuable if simpler integral models (see Sec. 4.1.1) are to be used, but they still give a good pointer to the generalities of a dense gas situation. An instantaneous release of volumetric size Q_0 can be considered passive if $(g_0' Q_0^{1/3})^{1/2}/U \leq 0.2$, while a corresponding limit for a continuous release of flow rate q_0 is suggested to be $(g_0 q_0/D)^{1/3} \leq 0.15$. It is worth noticing that for one of the trials used in this work, Thorney Island trial 21, $(g_0' Q_0^{1/3})^{1/2}/U = 3.1$, and could therefore safely be regarded as a "dense gas release" in this respect.

Different Richardson numbers are in general used in a lot of applications concerning dense gas dispersion. The Richardson number based on the wind's friction velocity, u_*, sets the diluting by the wind's turbulence in relation to the plume's stabilization by buoyancy related stratification. This Richardson number is usually expressed as (Rottman *et al.*, 1985*b*)

$$\mathrm{Ri}_* = \frac{g'h}{u_*^2}. \tag{2.3}$$

If the stabilization caused by the negative buoyancy force, noted by $g'h$, is much larger than the turbulence's diluting effect, u_*^2, resulting in a $\mathrm{Ri}_* \gg 1$, the plume will have well-defined, high-gradient edges. For the other extreme, a $\mathrm{Ri}_* \ll 1$, the plume will be very diluted and diffuse around the edges. One effect of a small Ri_* is that gas concentrations can be detected at a higher altitude than in the highly stratified case of a large Ri_*.

Description of the flow around geometries are best characterized by the Reynolds number. For flow around a cylinder, the Reynolds number is expressed as

$$\mathrm{Re}_D = \frac{UD}{\nu}, \tag{2.4}$$

where D is the cylinder's diameter and ν is the molecular kinematic viscosity. The Reynolds number is a parameter that "[correlates] the viscous behavior of all Newtonian fluids" (White, 2006, p. 27). Flows with very low Reynolds numbers are called *creeping flows*, Reynolds numbers in the middle range are *laminar* and high Reynolds number are most often *turbulent flows*. The gravity-driven slumping of dense gas is such a turbulent flow, as is the air flow around a container.

The turbulence in a slumping dense gas cloud is, however, separate from that of the atmospheric boundary layer surrounding the release source. This is important since the internal turbulence of a cloud will be stabilized as the flow spreads along the ground, a flow with energy spectra distributed over different ranges than that of the atmospheric flow. Energy spectra are described further in Sec. 6.4.

A leakage from an LNG storage tank is a typical dense gas release scenario. The LNG will initially spread along the ground and evaporate rapidly. This vaporization introduces a dense gas to the flow field around the storage tank. The Reynolds number of this flow can be used to describe the wake around the cylinder. For a high Reynolds number, which would typically be the situation with velocities and diameters in the orders of meters per second and meters, there will be a complex wake in the downstream zone of the cylinder, and the dense gas will initially settle into a recirculation zone.

Now, consider a case where the initial Richardson number, Ri_0, is large. The ambience (i.e. the wind field) will have little effect on the immediate spreading, but the already established wind field will have created a low-pressure zone on the sides of the cylinder (this can be seen with potential flow description). While the wind itself will not dilute or disturb the gas, to this the Richardson number is too large, the gas will flow into the low-pressure zones and shape what will look, from above, like a horse-shoe.

This example is included merely to emphasize how complex releases into the atmosphere can be, while still including only a few parameters.

2.1.2 Stationary dense gas

Britter (1989) gives four categories of dense gases. Each of these could be the topic of one thesis, and some effects from most of them are neglected in the work done here. The four categories can be summed up as follows:

1. Gases with higher molecular weight than the surrounding air;

2. gases with a lower molecular weight than the surrounding air, but with a relatively low temperature, resulting in a higher density;

3. gases with droplets, which increase the gas cloud's density. The droplets are often a result of the release scenario; and

4. gases which react with the water in the atmosphere resulting in a heavy composition.

These categories are incomplete whereas they do not mention one important aspect, namely the surrounding wind field. As shown through dimensionless quantities, the surrounding air flow determines many of the key parameters of a dense gas release. The surroundings have to be included even for a qualitative description of the dense gas flow. This is analogous to g' being an insufficient parameter for describing a release.

2.1.3 Dense gas flow

There are two extremes for the time aspect of a dense gas release, these being instantaneous or a continuous releases. The flow phenomena described in this section applies to an instantaneous release. The same characteristics will be present

for a continuous release as well, but such a release will sooner or later reach a steady state where the release and dilution processes are in equilibrium.

A released dense gas will develop through different phases. If the buoyancy force working on the gas is orders of magnitude larger than the advective force from the surrounding wind, the release's initial spreading will be radially symmetric outwards. While there is some mixing at the air-gas interface, most of the gas ends up undiluted in a ring around the edge of the cloud. The gas ring has a slightly elevated edge and air is entrained beneath this edge. This is one of the two main mixing zones in the initial spreading (Peters *et al.*, 1996). It is also worth noting that Rottman *et al.* (1985*a*) mark the establishing of this vortex ring as the end of the initial, slumping phase of an instantaneous dense gas release.

The other main zone occurs due to Kelvin-Helmholtz instabilities. Kelvin-Helmholtz instabilities can appear when there is a shear due to velocity discontinuities between fluids of different densities. Funada & Joseph (2001) outline how such instabilities are complex and dependent on a large scale of flow properties, from the fluids' surface tensions to the geometries of the surfaces. For a gravity-driven dense gas release, Kelvin-Helmholtz instabilities grow as waves over the top of the outer ring and make a second mixing zone in this ring's wake. Both of these zones are depicted in Fig. 2.1. The second phase of a release ends as the vortex ring collapses.

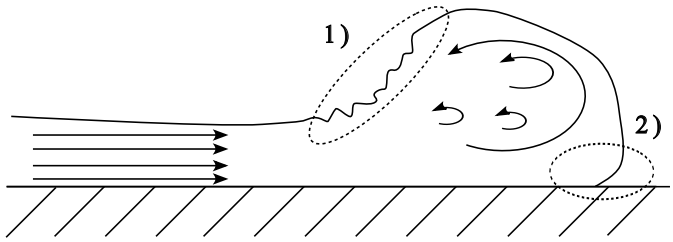

Figure 2.1: A sketch of the dense gas flow profile. The zone marked with 1) is the Kelvin-Helmholtz region, while the elevated nose is labeled 2).

After the collapse of the vortex ring, a more or less uniformly concentrated layer is left. The gravity is still what drives the flow, and in this phase most diluting of the cloud is done through the upper surface, by the turbulence in the wind, meaning that the atmospheric and turbulence properties affect the release of a dense cloud substantially.

This final phase of a dense gas flow is by far the largest in both time and space. Therefore, simpler models are often meant to describe the flow after the collapse of the vortex ring.

A non-reacting gas will remain even after this "final" phase, but it is now so diluted that its movement is determined entirely by the wind.

2.1.4 A typical release scenario

LNG spills are some of the most obvious examples of dense gas releases. Over a relatively large period—depending on the size of the storage tank—the liquid will vaporize and be a continuous source of dense gas. The gas will be of Britter's (1989) second category, gases with a lower molecular weight than the air, but a higher density due to low temperature. This gas will follow the described flow development, while being heated by the air and the surface, thus changing in its buoyancy characteristics. As the gas is advected by the wind, its dependency on the wind will increase and in a zone downstream the gas will follow the wind's motion almost perfectly. Summed up, an LNG spill will actually go through phases of negative, passive and *positive* buoyancy, since the gas' density decreases past the wind's as it is being heated.

As the LNG is spilled, it might also show instantaneous effects, where large transients are introduced to the flow field.

These occur through rapid phase transitions (RPT), where the LNG reaches its superheat limit (thermodynamic stability limit), it can no longer maintain its liquid form and it suddenly flashes to vapor. All this is because of mixture effects in the boundary layer close to the surface (Melhem *et al.*, 2006). These RPTs will create high pressure waves that propagate into the flow field with a high velocity, and they are therefore hard to model accurately.

2.2 Influence of surroundings

The descriptions to this point have been for a dense gas flow over a smooth flat surface. A brief description of dense gas flows over non-idealized surfaces are provided in this section.

2.2.1 Obstructions

For dense gases flowing over surfaces where the topographical features are large enough to be an actual obstruction to the flow (i.e. not just a "felt" surface roughness), one of two things can happen. The flow might behave as if it is encountering an inclination, or it might be confined by the obstacle.

A dense gas flowing down a hillside gains momentum as the potential energy is converted to kinetic energy—as for any other gravitationally propelled mass—giving a faster, lower cloud. In the opposite scenario, a gas flowing up an inclination, the resulting cloud will be taller and slower than one flowing over a flat surface. Simple models have been made for these sorts of flows, where assumptions about the surface are made in addition to the gas flow being in the final phase. Most notable of these models is the one of Webber *et al.* (1993), but even in this model the surface roughness is neglected and entrainment of air is left out, resulting in erroneous prediction of the cloud's movement.

If the flow reaches an obstacle like a fence or a wall, the gas can either be confined or it can flow over it, depending on the clouds height relative to the obstacle's. For a gravity-driven flow it can be shown through hydraulic analysis

that a dense gas cloud can surmount an obstacle about twice its height. The assumptions in a hydraulic analysis (e.g. no vertical movement) are in this case so substantial that this is a highly approximate relation.

2.2.2 Surrounding wind

Figure 2.2 shows the effect of changing one of the main wind model parameters, the roughness scaling height (more in Sec. 3.3). The simulation is done with Kameleon FireEx. The graph presents the gas concentration development just upwind of an impenetrable, five meter tall fence, at measuring point 1 (see Fig. 6.1, p. 46).

As will be seen in later results, the buoyancy modeling in KFX dampens the turbulence in the cloud substantially, and the gas is transported more through advection by the wind's mean velocity. The graph shows that increasing the turbulence level in the lower layers of the wind field, amplifies the dispersion of the gas over the fence. The two scaling heights, $z_0 = 0.0002$m and $z_0 = 0.1$m, correspond to open sea and tall grass, respectively. The fact that altering the turbulence level close to the ground has this effect, knowing that turbulence is not the main driving force at this stage, lays emphasis on how important it is to have an accurate modeling of the wind field.

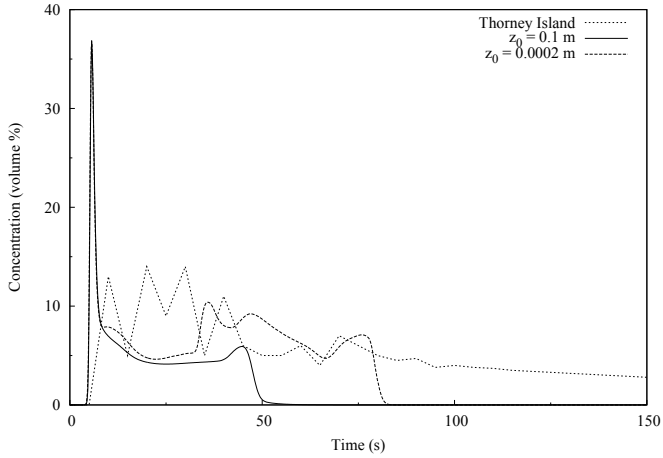

Figure 2.2: The effect of changing the scaling roughness height, z_0, at measuring point 1 (Fig. 6.1).

The figure is not included here as a scientific contribution, but rather to give perspective on why accurate modeling of the wind field is of such importance, it affects the dispersion more than almost any other parameter.

Consider the relation proposed by Briggs *et al.* (2001), where the vertical entrainment velocity w_e—which quantifies the clouds entrainment of air, and therefore its local dilution—is assumed proportional to u_*, the friction velocity at the

surface. This relation also includes Ri_* and is expressed

$$w_\mathrm{e} = \frac{0.65 u_*}{1.0 + 0.2\mathrm{Ri}_*}. \tag{2.5}$$

The planetary boundary layer is described in more depth in the next chapter.

2.2.3 Roughness

As is seen in the previous section, changing the turbulence level in the wind close to the ground affects the dispersion of dense gas. This small parameter study only adjusts the roughness scale in the *wind*, which means that the dense gas still feels the same surface. In cases with higher roughness, such as vegetation or rocky surfaces, the roughness itself might halt the flow. More likely, however, is it that the roughness alters the flow field through changing the turbulence levels and near-surface velocities of the wind. The descriptions provided in the prior section is thus still valid here.

McQuaid (1985) comment that the Grass present in the Thorney Island trials, had an aerodynamic height of 10–20 mm. At the time, "heavy gas dispersion models [were] not generally sensitive to z_0," and control of this parameter was not emphasized during the trials. However, dense gas releases may be affected by surface roughness in other ways than just turbulence. With a rough, semi-penetrable surface, the gas may be withheld in the roughness, and released gradually. This might explain why the experimental data shows presence of gas for a much longer period, the gas was absorbed in the grass, and seeping out for a longer period.

2.3 Hazardous concentrations

One of the main explanations for the process industry's sharp focus on dense gas dispersion is such gases' often hazardous nature. This section provides a short description of two main categories of dense gases, namely flammable and toxic, and states the main parameters of interest.

Fluctuations in the concentrations can change the hazard ranges, as described towards the end of the section.

2.3.1 Flammable gases

With more and more industrial resources being spent on liquefaction of natural gas (LNG) (BP, 2010), accidents involving such liquids are naturally also a point of interest. An LNG spill into atmospheric conditions will boil and vaporize rapidly, and a denser-than-air gas cloud will materialize.

A flammable gas diluted in air has a lower and upper flammability limit (LFL and UFL). Main zones of interest when considering such spills are therefore the development of these limits, and how far away from the spill the cloud is safe from igniting.

The high methane concentration in natural gas (often about 90–95% by mole) indicates that it is mainly methane's LFL that controls the cloud's LFL. In a

standard atmosphere, the LFL of methane is fairly low, $\sim$ 5% by volume, but due to the very low temperature the cloud can often still be considered negatively buoyant (Luketa-Hanlin *et al.*, 2007).

Luketa-Hanlin *et al.* (2007) also note how the atmospheric conditions affect the distance to the LFL. A stable atmosphere and low wind speeds result in the farthest LFL range, since buoyancy, low drag and small turbulence related dilution all increase the distance with higher concentrations, thus expanding the hazard zone.

2.3.2 Toxic gases

When the released denser-than-air gas is toxic it is important to know both the concentration levels and the time variation to estimate the effects of exposure (Britter & McQuaid, 1988). A toxic gas is disproportionately dependent on the concentration, meaning that a high concentration for a shorter time period is more harmful than a lower concentration for a longer period. This non-linearity impacts how the gas is modeled, and how the harm-level is assessed. It also emphasize the importance of correct flow modeling, as a good turbulence model would better show the distribution of the gas field and the transport of this.

In contrast to a flammable gas, which is often still considered "dense" in its LFL-state, a toxic gas might be just as harmful when its concentration is in the order of parts per million (ppm), meaning that it may as well be modeled as a neutrally buoyant gas (Britter & Griffiths, 1982). This is a less important aspect if the release is modeled with CFD (see Sec. 4.1.1), but when integral (or "box") models are the alternative, it eases the computation if the characteristics of a dense gas can be left out.

2.3.3 Concentration fluctuations

Both the effect of flammable and toxic gases are highly determined by how the concentrations fluctuate over time. For a flammable gas, where the hazard zone is often scaled by the LFL, one could have a mean concentration in the entire flow field which is lower than the LFL, but a fluctuating, intermittent area where the concentration is higher. An ignition in such a zone could propagate through the flow field, as long as the concentration fluctuations allow it. Such a type II error in a calculation could have severe results.

Fluctuations are of importance when assessing harm levels of toxic gases as well. Since a positive fluctuation would add disproportionately to the mean exposure of an individual, the toxicity models need to include a safety-factor which increases for more intense turbulence.

In a turbulent flow field, velocities, mass fractions, temperature and other flow characteristics have highly fluctuating values. The processes that determines this are stochastic and to know accurately how a flow field looks *a priori* is almost impossible. Think of meteorology, where a small adjustment in the initial conditions for the calculations can have a butterfly effect on the entire solution, and what was

announced to be a sunny, clear-skyed spring rains away. Figure 2.2 shows the impact of adjusting one wind parameter, and it seems justifiable to say that it is just as important that the turbulence model handles the wind field accurately, as good modeling of the dense gas itself. This surrounding atmosphere is described more thoroughly in the following chapter, before the k-ε turbulence model is introduced in Ch. 4.

2.3.4 The gas used in this thesis

In the rest of the work in this thesis, the specific hazardous effects of many dense gases are not considered. The focus is on the flow phenomena that differentiate a dense gas release, not their material related effects.

A similar assignment, which may have a foundation in the work done here, could be to study the development of a more specific problem. This could be to include the vaporization models and model an entire LNG spill accurately.

3 The atmospheric boundary layer

Luketa-Hanlin *et al.* (2007) define the planetary boundary layer as "the layer in which the Earth's surface affects the atmosphere through momentum, heat, and moisture exchange occurring over time scales of a few hours to less than a day."

As stated in the previous chapter, the wind field is a major contributor to the flow development of a gas release, and modeling this wind field accurately is important when simulating gas dispersion. Even if the dense gas initially is more or less unaffected by the surrounding wind, it will follow the wind's movement closely farther downstream. In order to get a realistic result for the length and width of a gas plume, and through that the LFL zone, it is important that the turbulence characteristics of the wind is correct throughout the domain.

This chapter gives a description of the atmospheric boundary layer and outlines the thermal and fluid processes that drives this. This lays the foundation for the chapter's last section, which is on one of the more used similarity models, the Monin-Obukhov theory.

3.1 Interactions between surface and air

If the radiative contribution of the atmosphere is neglected, the Earth's surface is where the energy from the sun is absorbed and enters its cycles. Depending on whether its daytime or night, hot or cold and the geometry of the environment, the surrounding air flow may show a vast number of behaviors.

The descriptions provided here are somewhat simplified and coarse, as the aim to lay a *sufficient* foundation for discussing simulation results in later chapters.

3.1.1 The near-surface energy budget

While the Earth receives energy from the sun by means of radiation, the Earth itself has a convective heat transfer with its surrounding atmosphere and a conductive heat transfer to and from the ground. Arya (2005) describes the energy budget near the Earth's surface. For a surface opaque to radiation, this can be expressed as

$$R_N = H + H_L + H_G, \tag{3.1}$$

where R_N is the net radiation from (positive into the surface) and H is the sensible heat transfer, H_L is the latent heat transfer and H_G is the ground heat flux to a sub-surface medium (all positive out from the surface).

The Earth's surface is seldom as "ideal" as that described by Eq. (3.1), especially are accident sites rarely both bare and flat. This implies that there are other things contributing in the heat exchange, such as vegetation and buildings. This is included by adding a term to Eq. (3.1) to get

$$R_N = H + H_L + H_G + \Delta H_s. \tag{3.2}$$

3.1.2 The adiabatic lapse rate

Before discussing the stability characteristics of an atmosphere, one important quantity must be defined: the adiabatic lapse rate.

An air parcel rising or declining in dry air without heat exchange with its surroundings (i.e. *adiabatically*) will experience a temperature gradient, $\partial\theta/\partial x_3$. This temperature gradient then defines the *dry adiabatic lapse rate*, γ, as

$$\gamma = -\frac{\partial\bar{\theta}_{\mathrm{ad}}}{\partial x_3}. \tag{3.3}$$

The corresponding temperature distribution is what is known as an adiabatic atmosphere. Air in different heights in the atmosphere often have temperatures which deviates from this distribution. Using the horizontal mean temperature of the adiabatic atmosphere, $\bar{\theta}_{\mathrm{ad}}$, this difference is expressed by $\vartheta = \theta - \bar{\theta}_{\mathrm{ad}}$.

3.1.3 Stability

The sensible heat portion, H, gives a temperature gradient in the air above the surface. An assumption used throughout this thesis is that the meteorological fluctuations occur over much larger scales than those present in the investigated scenarios. Therefore, there are no gradients in the lateral directions and thus the temperature gradient is in the vertical direction only, which is also a standard assumption for similarity theories.

On a fairly short time-scale (seasonal variations not considered), the surface fluxes go through a diurnal variation (Arya, 2005). During the day, the surface is heated by the sun, and the air receives heat from the surface, $H > 0$—remember, radiative contribution of the atmosphere is neglected. This heats up air parcels, giving a $\vartheta > 0$, and the buoyancy drives the air upwards. The wind-field is "unstable" due to Rayleigh-Taylor instabilities between the now heated, lower gas and its surroundings. Now buoyancy effects cause a production of turbulence and there is substantial mixing throughout the boundary layer, what is called a "convective layer" or "mixing-layer". One characteristic feature of such layers are their almost uniform velocity distribution (Arya, 2005). This occurs due to the very effective transport of momentum in a turbulent flow.

In the night, typically, there is a radiation-related loss of heat from the surface $R_N < 0$, meaning that the air provides heat to the ground, $H < 0$ (neglecting the often substantial condensing of water vapour H_G, an assumption that does not inflict with the argument). Now $\vartheta < 0$, close to the ground, and the heaviest gas is that flowing closest to the surface. This *stratification* of the boundary layer is

characteristic for a stable atmosphere. In this scenario the negative buoyancy the air "feels" gives a damping of turbulence related fluctuations.

In between these settings, there are critical points where $\vartheta = 0$ and $\partial\vartheta/\partial x_3 = 0$. In this *neutral* atmosphere, a displaced lump of air would remain in its new position, due to the local uniform density. Correspondingly, it would rise in an unstable atmosphere and descend in a stable atmosphere.

3.1.4 Buoyant vs. shear production of turbulence

As mentioned in the previous section, a buoyancy-driven turbulence production occurs due to heat transport through the surface layer. Comparing this production term to a more typical shear-related production, can be expressed by a Richardson number (introduced in Sec. 2.1.1). This *flux Richardson number* is defined as (Tennekes & Lumley, 1972, pp. 98–99)

$$\mathrm{Ri}_f = \frac{g}{\overline{\theta}_{\mathrm{ad}}} \frac{\overline{u_3'\theta'}}{\overline{u_1'u_3'}\partial\overline{u}_1/\partial x_3}, \tag{3.4}$$

where θ_{ad} is the mean temperature of an adiabatic atmosphere, $\overline{u_3'\theta'}$ is the turbulence related heat flux, and $\overline{u_1'u_3'}$ is the turbulence related stress ($\overline{u_1'u_3'} < 0$), or momentum flux. $\partial\overline{u}_1/\partial x_3 > 0$, typically.

Tennekes & Lumley (1972) explain that an upward-directed turbulence related heat flux, $\overline{u_3'\theta'} > 0$, generally corresponds to $\partial\vartheta/\partial x_3 < 0$. This implies a $\mathrm{Ri}_f < 0$, and the production of turbulence is done through both buoyancy and shear effects, which means that $\mathrm{Ri}_f < 0$ corresponds to an unstable atmosphere.

For the case where $\mathrm{Ri}_f > 0$, the heat flux is downwards ($H < 0$) and the atmosphere has a stable stratification. Now the buoyancy works to dampen the turbulence, and above a critical flux Richardson number, Ri_{fc}, (estimated to lie between 0.25 and 0.5 (Arya, 2005)) turbulence only occur intermittently and cannot be maintained (Tennekes & Lumley, 1972).

For a neutral atmosphere, the temperature distribution follows the adiabatic lapse rate perfectly, and $\partial\vartheta/\partial x_3 = 0$. This also means that $\mathrm{Ri}_f \approx 0$, and buoyancy neither produces nor dampens turbulence in the atmosphere.

3.1.5 Focusing on neutral and stable atmospheres

The modeling of convective ABLs contains a number of difficulties that are not present when modeling a neutral or stable boundary layer. As the unstable situation can result in substantial movement and large turbulent eddies even in an otherwise still atmosphere, it is harder to find a coherent model for such flows. The simulations in this thesis are therefore of either neutral or stable atmospheres, with the sharpest focus on maintaining a neutral atmospheric boundary layer through a large calculation domain.

Daytime scenarios often introduce an unstable flow, and there is then an incentive also to have focus on convective boundary layers in future revisions of the models tested in this thesis.

3.2 Layer-wise description

For the atmospheric boundary layer, five idealized layers can be defined (Mahrt, 1999). These are the roughness sublayer, the surface layer, the "local scale" layer, the "z-less" layer and the boundary layer top.

How these layers are correlated with the stability is depicted in Fig. 3.1. The z-dependency occurs over a shorter region when the atmosphere becomes more stable.

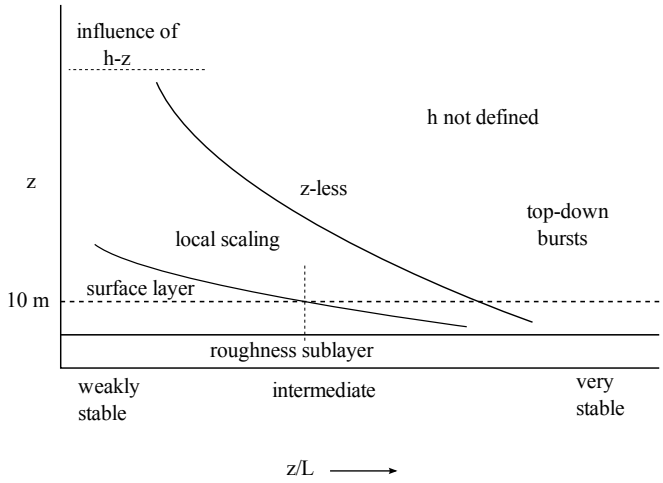

Figure 3.1: The stability regions, adapted from Mahrt (1999, Fig. 1) (not to scale)

The two following layer descriptions include a stability parameter based on the Obukhov length, L (Obukhov, 1971). This derived stability parameter, z/L, is formally introduced in Sec. 3.3. Figure 3.1 shows how the stability increases with increasing z/L. At one height, the local stability therefore increases with decreasing values of L.

3.2.1 Roughness sublayer

In this layer the time-averaged flow components vary spatially over the roughness elements, and it seems unachievable to find a similarity solution for the gradients and fluxes. One can think of this layer's contribution as the ΔH_s term in Eq. (3.2).

Luketa-Hanlin *et al.* (2007) mention a work-around for this problem. If the roughness elements are of a substantial height (e.g. small buildings or trees), a "roughness height" is calculated (typically 80-90% of the obstacle heights) and the new ground level is placed at this height.

3.2.2 Surface layer

For a flat, smooth surface, the surface layer will have fluxes and gradients that are numerically similar to those on the physical surface. The height of this layer

is dependent on z/L (see Fig. 3.1). It is a common assumption that all fluxes are constant throughout the surface layer, an assumption that is important when models for the surface layer are derived.

The Monin-Obukhov similarity theory (described in Sec. 3.3) is only valid for this surface layers. Therefore, most calculations done for this thesis are done with a domain which would, if entirely realistic, contain only the surface layer. Nevertheless, for coherence, the upper layers are also included here.

3.2.3 Local scaling layer

Above the surface layer, lies the local scaling layer, where the approximation of height independent fluxes becomes invalid (Mahrt, 1999). While the typical Obukhov length L is based on the surface fluxes (i.e. not local for a $z \neq 0$), one can define a new length scale Λ which is calculated by local fluxes.

It has not yet been found a consistent height-dependency of the fluxes, and it is therefore difficult to find coherent models for this layer. For numerical calculations, where the top of the domain is defined by the user, this often means that calculations yield results as if the surface layer stretched farther than it actually is, as the local scaling layer is probably not defined in the software's wind boundaries.

3.2.4 Z-less layer and the boundary layer top

At even higher z or z/Λ values, many quantities are independent of z/Λ, what is often called z-less stratification (Arya, 2005). It can be viewed as the limit where functions of z/Λ approach constant values. Pahlow *et al.* (2001) notes how the concept of z-less stratification "implies that the turbulent eddies are no longer directly influenced by the surface as the atmosphere becomes very stable."

As all quantities approach constant values and z is near the boundary layer top h, the distance from this top $h - z$ might be a more suitable length scale. The stability parameter for this region would then be $(h - z)/\Lambda$.

3.2.5 The very stable regime

As the stability in the atmosphere increases, the height of the layers are expected to decrease. As seen in Fig. 3.1, this results in an earlier transition to z-less stratification, and surface layer models such as Monin-Obukhov might therefore not be usable.

3.2.6 The convective, unstable boundary layer

As mentioned, one main difference between the classes is that the stable boundary layer is driven by the shear from the free wind, and a dynamic flow field is thus dependent on having such free wind. In the unstable, or convective, boundary layer, however, there can be movement and "wind" due to the free convection and positive buoyancy alone (Stull, 1988).

3.3 Monin-Obukhov similarity theory

Monin & Obukhov's (1954) similarity theory was proposed in 1954, and derived to answer some of the "number of debatable questions in the theory of surface-layer mixing." It is a similarity theory, therefore using appropriate scaling parameters to define the flow field for the constant flux surface layer (Arya, 2005).

3.3.1 Scaling parameters

A first assumption is that both the momentum and heat fluxes are constant throughout the surface layer. Then the turbulence related heat flux is expressed (comments on notation in Ch. 4)

$$\overline{u_3'\theta'} = \frac{H}{c_p\rho} = \text{const.} \tag{3.5}$$

and the turbulence related momentum flux is

$$-\overline{u_1'u_3'} = \frac{\tau}{\rho} = u_*^2 = \text{const.}, \tag{3.6}$$

where an additional assumption is that the turbulence related transport is dominant. This led Monin & Obukhov (1954) to the Obukhov length L and temperature scale θ_*, which are defined as

$$L = \frac{-u_*^3}{\kappa\frac{g}{\theta_{\text{ad}}}\frac{H}{c_p\rho}} \tag{3.7}$$

and

$$\theta_* = -\frac{1}{\kappa u_*}\frac{H}{c_p\rho}. \tag{3.8}$$

Where a negative heat flux, $H < 0$, (a stable stratification) corresponds to $L > 0$ and $\theta_* > 0$ and a positive heat flux, $H > 0$, (or an unstable atmosphere) gives $L < 0$ and $\theta_* < 0$. κ is von Karman's constant, usually $\kappa \approx 0.4$.

3.3.2 The implementation in KFX

Notes must be made on the implementation of this similarity theory in KFX, as some simplifications are made.

A typical, logarithmic velocity profile is used, namely (Van Ulden & Holtslag, 1985)

$$u = u_*\frac{1}{\kappa}\left[\ln(z/z_0) - \psi_M(z/L) + \psi_M(z_0/L)\right], \tag{3.9}$$

where ψ_M is an integrated similarity function for the momentum,

$$\psi_M = -17(1 - e^{-0.29z/L}). \tag{3.10}$$

z_0 is the roughness scaling height, which in effect is a displacement height. The

function ψ_M is more formally derived through a similarity function, ϕ_M, via

$$\psi_M = \int_{z_0}^{z} \left(\frac{1}{z} + \frac{\phi_M}{z} \right) dz, \tag{3.11}$$

where the empirically determined stability function $\phi(\zeta = z/L)$ origins from a modification to the constant shear layer equation, $\partial\bar{u}/\partial z = u_*/(\kappa z)$ (which fits best for a neutral atmosphere). This modified equations is expressed

$$\frac{\partial \bar{u}}{\partial z} = \frac{u_*}{\kappa z}\phi_M(\zeta). \tag{3.12}$$

The similarity function for stability is typically on the form $\phi_M = A+B\zeta$, for $\zeta \geq 0$. This does not directly result in the relation for ψ_M used in KFX, Eq. (3.10), which then is an entirely empirically based function.

The temperature potential is calculated in a similar manner by

$$\Delta\theta = \theta_* \left[\ln(z/z_2) - \psi_H(z/L) + \psi_H(z_2/L) \right], \tag{3.13}$$

where z_2 is a reference height for the heat flux.

In KFX, and what is common engineer application practice, however, the user provides L directly, based on empirical data, while the temperature field is assumed uniform. This assumption is not necessarily that grave. It does nevertheless amplify the incentive to use a neutral atmosphere in the modeling. Using a height-varying temperature field is a suggested topic for future work, coupled with investigation of the effect of buoyancy in the turbulence modeling.

Chapter 4 will see to the proper introduction of two important turbulence related quantities, k and ε (the mean turbulence kinetic energy and the dissipation rate of this, respectively). Suffice to say here, in KFX these are initialized by the relations given by Huser *et al.* (1997), that is

$$k = \frac{u_*^2}{\sqrt{C_{\mu 1}}} \left(1 - \frac{z}{h} \right)^2 \tag{3.14}$$

and

$$\varepsilon = \frac{u_*^3}{\kappa} \left(\frac{1}{z} + \frac{4}{L} \right). \tag{3.15}$$

The boundary layer height, h, is found to be approximated by (Duynkerke, 1988)

$$h = 0.4 \left(\frac{u_* L}{f} \right)^{1/2}, \tag{3.16}$$

where f is the Coriolis parameter, and is related to the rotational speed of the Earth, Ω, and latitude, φ, through $f = 2\Omega \sin\varphi$. For a latitude of 60°, $f \approx 1.26 \cdot 10^{-4}\,\mathrm{s}^{-1}$. With wind shear velocities of $u_* \approx 1\,\mathrm{m/s}$, this means that the boundary layer height varies from the order of 10^3 m down to the order of 10^2 m for neutral and stable atmospheres respectively. Since the surface layer, where similarity theories

are meant to be valid, stretch to about 10% of the entire boundary layer height, the Monin-Obukhov theory should ideally not be used in calculation domains higher than a few tens of meters, depending on the atmospheric stability.

Pahlow *et al.* (2001) conducted a number of experiments attempting to find statistical validity for the Monin-Obukhov relations. By scaling the dissipation rate of mean turbulence kinetic energy, ε, with $u_*^3/\kappa z$, a "generally accepted prediction form of the normalized average dissipation rate is ϕ_ε being proportional to the stability parameter,"

$$\phi_\varepsilon = A + B\zeta. \tag{3.17}$$

This is of the form already used in Eq. (3.15), where A, as is common practice, is one. Pahlow *et al.* (2001) found, however, that when approaching the neutral limit, $\phi_\varepsilon \neq 1$, or more precisely

$$\lim_{z/L \to 0} \phi_\varepsilon = 0.61. \tag{3.18}$$

This is, as said, not common engineering practice, nor is the value of B uniquely determined, the standard value in both KFX and used by Luketa-Hanlin *et al.* (2007) is $B = 4$, while some results show a tendency towards $B = 5$ (Pahlow *et al.*, 2001). Han *et al.* (2000) also use meteorological data to find the form of the model constants, and for the neutral regime they end up wind $A = 1.24$ and $B = 4.3$, which is closer to that used here. The research is, characteristically, not conclusive.

What is certain is that most of the production of turbulence kinetic energy by shear in the flow occurs close to the surface. The explanation for this is that shear-driven production in a boundary layer is of the form $P \sim (d\bar{u}/dz)^2$ (more in Ch. 4), and the velocity gradient, $d\bar{u}/dz$, is largest close to the surface. Assuming local equilibrium (i.e. $P = \varepsilon$, neutral atmosphere), both P and ε take high values in the region close to the surface.

It is apparent that some of the results found in this thesis can be due to incorrect or inaccurately inserted boundary conditions. The hope is, nevertheless, that minute adjustments to the boundary conditions would not result in a significant change in the outcome, and that the same development would be seen throughout the calculation domain. There will always be a number of explanations for why the results are as they are, and what could be done to change their appearance. Throughout this work, A is kept at one, and $B = 4$. One suggestion for future work could be to investigate the validity of these values further.

3.3.3 Critique

McNaughton (2009) states that

> there seems to be no alternative to similarity modeling. Fortunately, atmospheric boundary layers, with their high Reynolds and Rayleigh numbers, seem particularly well suited to this approach. The key is to find the right set of basic variables and the right way to use them. This involves choosing the right conceptual model.

He does not, however, feel that the Monin-Obukhov similarity theory is the right conceptual model. Since the work leading to the Obukhov length, L, is originally based on Prandtl's mixing length model (Obukhov, 1971) it does not capture the higher order statistical moments, as the peaks in for instance temperature spectra in the surface layer no longer vary over the turbulence wavenumber. McNaughton (2009) argues that as this similarity theory is meant to be expressed through local parameters, it still relies heavily on the height, which is the difference between the current position and the ground level, and therefore a non-local quantity.

However, as is even noted by McNaughton (2009), "the real test is whether the theory can reduce experimental data to universal constants or relationships. In this the [Monin-Obukhov] scheme can work reasonably well, if not perfectly." This is an important note to remember when considering the simulation results later in the thesis, the boundary conditions themselves are not *perfect*, but are more than likely good enough for the typical engineering applications.

4 Modeling

The map is not the territory

—Alford Korzybski

To better understand the world around us, there have been developed models with a vast span of applications and purposes. The sun can be modeled as a circle with straight lines going radially outwards in a child's drawing, while experimental physicists take a more theoretical approach. These are both *models*, albeit of different sophistication.

This chapter contains a quick overview of the different solution paths to modeling dense gas releases, with an emphasis on one of the most popular turbulence models, the k-ε model.

4.1 Scales and model hierarchy

Before delving into the turbulence model that is in focus here, the k-ε model, it could be useful to know how dense gas models have developed and matured over time, and what approaches are in use today. The first section is included to give an appreciation of the hurdles a dense gas model has to overcome.

4.1.1 The range of scales

In a transient simulation of a large scale dense gas release, there is a number of physical scales involved. In the period shortly after the gas is released, the high density gradients will distinguish it as a dense gas release by prohibiting dilution of the gas. A neutrally buoyant gas would "follow" the wind field's turbulence related transport of mass. In contrast, a release with a high Richardson number will continue as if unaffected by the turbulence in the wind field in an intermediate period after the slumping phase. The transport of the gas is then due to mean convection by wind and the gas' own gravity current.

As the gas is distributed over a larger area, its average concentration decreases, and behavior due to density differences diminish. The gas will now have a significant dispersion by turbulence driven effects as well, and correct modeling of these will be important. The cloud is by now a long distance from its release point, and the total domain of interest may have length scales in the order of kilometers.

Therefore, there are a range of physical quantities and scales to be considered when modeling dense gas releases. The accuracy of these estimates determines the

validity of the modeling. In the close range, the way density gradients influence dense gas dispersion by turbulence is one point of focus, while in the far field it is important to have an accurate description of the wind's turbulence field.

This dichotomy, the close field's density effects and the far field's influence by turbulence, is important to remember when deciding on a dense gas model.

4.1.2 Integral models and shallow water equations

In an integral model, the properties of the entire cloud are integrated, and only simple ordinary differential equations describing the movement of the cloud as a whole are left to be solved. These models apply to the phase after the collapse of the outermost vortex ring (see Sec. 2.1.3), and it is assumed that all dilution happen through the upper surface of the cloud.

While these models are easy to solve for even weaker computers, there is a drawback that leaves them almost useless today; they are almost exclusively for idealized situations, that is to say no obstructions in the flow field, and simple ambient conditions. These models are also referred to as "box models".

In shallow water equation (SWE) models, the flow properties are averaged in the vertical direction (or along the gravitational field). This leaves momentum equations for the lateral directions. SWE-based models are not extensively used for dense gas dispersion, but they can be beneficial when results are needed quickly, as in the case of an emergency (Brambilla *et al.*, 2009).

Another use for SWE models, is the spreading and flow of liquids. It is then possible to get a fairly accurate description of an LNG spill and its range (Lilleheie, 2011). Other models may then handle the dispersion of dense gas as the liquid evaporates.

4.1.3 Computational fluid dynamics

Computational fluid dynamics (CFD) is defined by Versteeg & Malalasekera (2007, p. 1) as "the analysis of systems involving fluid flow, heat transfer and associated phenomena such as chemical reactions by means of computer-based simulation." This does not seem to exclude the already discussed integral models, but the term is still conventionally used for models based on the Reynolds-averaged Navier-Stokes (RANS) equations. An argument could also be made on the use of the word "simulation" in the definition referring to the "higher-level" RANS models, while the solving of simpler relations could be termed "modeling", but linguistics is not the topic of this thesis.

CFD models are based on the Navier-Stokes equations. Depending on how these are treated, the resulting model is placed in one of the categories described here. RANS models use time-averaged Navier-Stokes equations, while the sub-grid phenomena are handled by turbulence models, such as the k-ε model. This has proved to be a well-suited approach for most engineering applications.

Next in the cascade is large eddy simulation (LES). In these models a much finer numerical grid is used, and the larger turbulent motions, or eddies, are solved directly with momentum equations. This means that most of the kinetic energy

and bulk motion are solved with transport equations directly. Finally sub-grid models are used for the smaller eddies, where most of the dissipation occurs, to also solve to properties not caught in the "filtering". As computers become more powerful, an increasing number of simulations are done with LES. Simpler RANS models still have an advantage over LES models in that they are easier to define boundary conditions for, the numerical solvers are often more stable and they are less computer demanding (Versteeg & Malalasekera, 2007, pp. 98–110).

If the grid is refined to the limit where even the smallest turbulent motions (i.e. the Kolmogorov scales) are "caught", there is no need for sub-grid models and all fluid properties and flow phenomena are preserved by solving un-filtered equations, this is termed direct numerical solution (DNS). DNS is extremely computer demanding, and is therefore almost only used in research related problems, since produces excellent data to test other turbulence models and statistical relations against (Versteeg & Malalasekera, 2007, p. 110).

4.1.4 Other approaches and testing

There are many other approaches to calculation of dense gas dispersion. Dedicated models (e.g. DEGADIS, SLAB and HEGADAS) can give as good results as conventional CFD, in less computational time. However, one of the key aspects of CFD is its diversity, in one single program it is often possible to solve a multitude of different problems, thus making it more apt for several applications.

It is also developed a form for evaluation of dense gas dispersion model, SMEDIS, where a developer can evaluate his or her dispersion model, based on some standardized criteria (Daish *et al.*, 2003).

Mitsubishi Heavy Industries has developed an numerical code called the STD model, which is a dispersion model for dense gas flow (Ohba *et al.*, 2004) using transport equations for probability density functions. This model is supposed to mitigate the problem of not covering the total hazardous area for dense gas releases, which is outlined in Sec. 2.3.3.

Ohba *et al.* (2004) used for this a finite difference method (see Sec. 5.2) to solve "the fundamental equations for velocity, concentration, gas density [...] and standard deviation of concentration as independent variables." The empirical constants which are bound to be a part of such expressions were found by comparing the STD model with empirical data and already validated data from a k-ε model simulation. A main source of errors were a time scale for dissipation, which again was calculated using a reference length for along-plume diffusion.

The simulation results from this model has proved encouraging. For simulations done with a structure in the flow field, erroneous result are accounted for by the calibration of the constants and what "may be an inherent limit of k-ε turbulence models in general," Ohba *et al.* (2004).

4.2 General equations

In this section some general relations, such as averaging and gradient models, are presented.

In the rest of this chapter, Einstein's summation rule is used unless otherwise stated. This means that a repeated index (e.g. i) implies summation over same index, and is used merely for the sake of brevity.

4.2.1 Averaging

When studying turbulent flows, it is common practice to consider the variables as having an average, quasi-steady component and a fluctuating, a view that is called Reynolds decomposition. This means that a time-varying flow variable $\phi(t)$ can be decomposed to

$$\phi(t) = \overline{\phi} + \phi'(t), \tag{4.1}$$

where $\overline{\phi}$ is the average component and $\phi'(t)$ the fluctuating component. The averaging done here is an un-weighted Reynolds averaging, or time-averaging, done through

$$\overline{\phi} = \frac{1}{\Delta t}\int_{t_0}^{t_0+\Delta t} \phi(t)\, dt, \tag{4.2}$$

which indicates

$$\overline{\phi'(t)} = 0. \tag{4.3}$$

In highly density-varying situations, for instance a combustion calculation, the averaging should be weighted against the density. This is called Favre averaging, and is done by

$$\widetilde{\phi} = \frac{\int_{t_0}^{t_0+\Delta t} \rho(t)\phi(t)\, dt}{\int_{t_0}^{t_0+\Delta t} \rho(t)\, dt} = \frac{\overline{\rho\phi}}{\overline{\rho}}. \tag{4.4}$$

Decomposition using Favre averaging is written

$$\phi(t) = \widetilde{\phi} + \phi''(t), \tag{4.5}$$

implying that $\widetilde{\phi''(t)} = 0$, but $\overline{\phi''(t)} \neq 0$.

4.2.2 The transport equation

Most fluid modeling utilizes *transport equations*. These are partial differential equations (PDEs), which, for a general scalar quantity ϕ, can be expressed as

$$\underbrace{\frac{\partial(\bar{\rho}\tilde{\phi})}{\partial t}}_{\text{I}} + \underbrace{\frac{\partial(\bar{\rho}\tilde{u}_j\tilde{\phi})}{\partial x_j}}_{\text{II}} = \underbrace{\frac{\partial}{\partial x_j}\left(\Gamma_{\phi,\text{eff}}\frac{\partial\tilde{\phi}}{\partial x_j}\right)}_{\text{III}} + \underbrace{\bar{\rho}\tilde{S}_\phi}_{\text{IV}}, \tag{4.6}$$

where the different terms are as follows:

I Transient term

II Convective term

III Diffusive term, including both molecular diffusion and diffusive effects caused by turbulence

IV Source or sink term for the property ϕ which includes effects that are not taken care of by the three previous terms

The use of the effective diffusion coefficient, $\Gamma_{\phi,\text{eff}}$, is common in turbulence modeling. It is defined as

$$\Gamma_{\phi,\text{eff}} = \frac{\mu}{\sigma_\phi} + \frac{\mu_t}{\sigma_{\phi t}}, \tag{4.7}$$

where σ_ϕ and $\sigma_{\phi t}$ are the molecular and turbulence related Prandtl-Schmidt number for ϕ, respectively. These are empirical parameters relating the diffusion of ϕ to the diffusion of momentum by molecular and turbulence related trans sport. An effective dynamic viscosity, μ_{eff}, can be expressed as the sum of the molecular and turbulence related contribution to the viscosity, $\mu_{\text{eff}} = \mu + \mu_t$. Finding μ_t is often the main problem in turbulence modeling, and its definition is accounted for later in this section.

There are a number of ways to solve for this parameter, and the one alternative suggested here is just that—*one* alternative. All models have their strengths and weaknesses, so the user is responsible for understanding the model and its areas of use.

4.2.3 The mass transport equation

For dense gas dispersion simulations, the most obvious scalar of interest is the mass fraction of the dense gas, a parameter that determines LFL zones and other hazard regions. After Reynolds decomposing, before using the transport model, the transport equation for this scalar quantity, Y for species l, is

$$\frac{\partial \bar{\rho}\widetilde{Y}_l}{\partial t} + \frac{\partial(\bar{\rho}\widetilde{u}_i\widetilde{Y}_l)}{\partial x_j} = \frac{\partial}{\partial x_j}\left(-\bar{\rho}\widetilde{Y_l V_{lj}}\right) + \frac{\partial}{\partial x_j}\left(-\bar{\rho}\widetilde{u_j'' Y_l''}\right) + \bar{\rho}\widetilde{R}_l + \bar{\rho}\widetilde{R}_{\text{liq},l}, \tag{4.8}$$

where ρ is the gas density, V_{lj} is the molecular diffusion velocity in the x_j-direction, R_l is a chemical source term and $R_{\text{liq},l}$ is a source term due to phase transition.

Using the transport model from Eq. (4.6) on Eq. (4.8) gives the more easily solvable

$$\frac{\partial \bar{\rho}\widetilde{Y}_l}{\partial t} + \frac{\partial(\bar{\rho}\widetilde{u}_j\widetilde{Y}_l)}{\partial x_j} = \frac{\partial}{\partial x_j}\left(\left(\frac{\mu}{\sigma_{\widetilde{Y}_l}} + \frac{\mu_t}{\sigma_{\widetilde{Y}_l t}}\right)\frac{\partial \widetilde{Y}_l}{\partial x_j}\right) + \bar{\rho}\widetilde{R}_l + \bar{\rho}\widetilde{R}_{\text{liq},l}, \tag{4.9}$$

where a gradient model (see Sec. 4.2.6) has been applied on the diffusive transport of Y_l.

4.2.4 The turbulence Schmidt number

In Eq. (4.9), the turbulence Schmidt number, $\sigma_{\widetilde{Y}_l t}$, is introduced. This is the ratio between turbulence related viscosity and turbulence related diffusivity, $\sigma_{\widetilde{Y}_l t} =$

$\nu_t/\mathcal{D}_{\widetilde{Y}_l t}$, and is most often set to be in the order of unity, or the value of the molecular Prandtl number. The molecular Prandtl number relates diffusion of momentum and heat, and is expressed $\mathrm{Pr} = \mu c_p/\lambda$, which for air has a value of 0.71.

This is typically not a problem for a neutrally buoyant gas release, seeing how the flow of the gas will directly follow the flow of the surroundings—at least after a transient period where it interchange momentum with the surrounding flow. In a dense gas release the situation is not as simple. Here the density gradient works to suppress movement of the gas with increased stability, while momentum can be transferred by other means, for example internal waves (Andronopoulos *et al.*, 1994). The effect of this is a possible underestimation of $\sigma_{\widetilde{Y}_l t}$, and therefore an overestimation of the turbulence driven dispersion.

Andronopoulos *et al.* (1994) used, in their simulation of Thorney Island trial 21, a turbulence Schmidt number that was dependent on the local stability. Ellison & Turner (1960) found that for a stable flow, as that in a dense gas cloud, the turbulence Schmidt number could be expressed as

$$\sigma_{\widetilde{Y}_l t} = \mathrm{Pr}\frac{(1-\mathrm{Ri}_f)^2}{1-\mathrm{Ri}_f/\mathrm{Ri}_{fc}}, \tag{4.10}$$

where Ri_f and Ri_{fc} are the flux Richardson number and critical flux Richardson number, as mentioned in Sec. 3.1.4.

To find Ri_f Eqs. (3.4.14) and (3.1.14) from Tennekes & Lumley (1972) are used, a use resulting in

$$\mathrm{Ri}_f = \frac{\mathrm{Ri}}{\sigma_{\widetilde{Y}_l t}}. \tag{4.11}$$

Ertesvåg (2000) notes that the Richardson number can be modeled as

$$\mathrm{Ri} = -\frac{g}{\rho}\frac{d\rho}{dx_3}\left(\frac{d\bar{u}_1}{dx_3}\right)^2, \tag{4.12}$$

if x_3 is directed against the gravitational acceleration, g. These equations give an implicit relation for $\sigma_{\widetilde{Y}_l t}$, and an iterative process must be applied for it to be used in a CFD code.

4.2.5 The momentum equation

After having decomposed and Favre averaged the Navier-Stokes momentum equation, the transport equation for momentum is expressed

$$\frac{\partial\bar{\rho}\widetilde{u}_i}{\partial t} + \frac{\partial(\bar{\rho}\widetilde{u}_i\widetilde{u}_j)}{\partial x_j} = -\frac{\partial\bar{p}}{\partial x_i} + \frac{\partial}{\partial x_j}\left(\bar{\tau}_{ij} - \bar{\rho}\widetilde{u_i''u_j''}\right) + \bar{\rho}\tilde{f}_i, \tag{4.13}$$

in which the source term is most typically the gravity, but in some instances a Coriolis force or—if rarely—a magnetic force. Nevertheless, what is specifically worth noticing in this equation is the Reynolds stress term, $-\bar{\rho}\widetilde{u_i''u_j''}$, which will be

returned to shortly ($-\rho\overline{u_i' u_j'}$ using Reynolds averaged quantities).

4.2.6 Gradient models

In Eq. (4.7), the diffusivity of a flow variable ϕ, was expressed in terms of its molecular diffusivity and a turbulence "diffusivity". Using the Boussinesq assumption, that the turbulence related transport of a variable is proportional to the mean flow gradient, as for molecular diffusivity, a simple gradient model can be derived to show the turbulence related fluxes. For the variable ϕ, such a model can be expressed

$$-\bar{\rho}\widetilde{u_j''\phi''} = \frac{\mu_t}{\sigma_{\phi t}}\frac{\partial\widetilde{\phi}}{\partial x_j}. \tag{4.14}$$

4.3 Turbulence modeling

In Eq. (4.13) a term for the Reynolds stresses, $-\bar{\rho}\widetilde{u_i'' u_j''}$, occurred. Hinze (1975, p. 23) stresses that the Reynolds stresses are, even if they appear as a stress on a macroscopic level, really "convective accelerations in the turbulent motion." Whatever definition, the task to solve in most turbulence model, is finding an adequate solution for these "stresses". This section presents one alternative to such a solution, the k-ε turbulence model, here in a version meant for highly density varying flows.

This section starts with the introduction of two k-ε models that use Reynolds averaged quantities, before it is described how the model is implemented in KFX.

4.3.1 The standard k-ε model

For a fluid with velocity u_i, its kinetic energy per mass is $\frac{1}{2}u_i u_i$ (remember Einstein's summation notation) (Ertesvåg, 2000, p. 48). After a decomposition, the term $\frac{1}{2}u_i' u_i'$ expresses the kinetic energy in the turbulent fluctuations. Averaging this leaves the *mean turbulence energy*, or k, which is expressed

$$k = \frac{1}{2}\overline{u_i' u_i'}, \tag{4.15}$$

whereas its dissipation to heat by molecular friction, ε, is

$$\varepsilon = \nu\overline{\left(\frac{\partial u_i'}{\partial x_j}\right)^2}. \tag{4.16}$$

Assuming that the larger, more kinetic energy-carrying eddies are independent of the molecular viscosity, which only has the turbulence related effect of dissipating the movement to heat, these Reynolds stresses can be modeled as

$$-\rho\overline{u_i' u_i'} = \mu_t\left(\frac{\partial\bar{u}_i}{\partial x_j} + \frac{\partial\bar{u}_j}{\partial x_i}\right) - \frac{2}{3}\left(\rho k + \frac{\partial\bar{u}_l}{\partial x_l}\right)\delta_{ij}, \tag{4.17}$$

where δ_{ij} is the Kronecker delta. In this relation, the Boussinesq assumption is made, namely that turbulence stresses are "directly proportional to the velocity gradients," as viscous stress is to the viscosity (Hinze, 1975, p. 23).

The k-ε model is a two-equation model, meaning that in addition to equations for the mean-field variables, the turbulence properties are calculated by means of two additional transport equations. The two transport equations are for the energy of the turbulence and the dissipation rate of this energy, k and ε, respectively. Depending on the application, these can be expressed in different forms.

4.3.2 High Reynolds number k-ε model

In a high Reynolds number turbulent flow, the diffusive transport of any flow variable is dominated by turbulence effects. Thus, the molecular viscosity can be neglected, and the transport equations for k and ε are

$$\frac{\partial(\rho k)}{\partial t} + \frac{\partial(\rho \bar{u}_i k)}{\partial x_i} = \frac{\partial}{\partial x_i}\left(\frac{\mu_t}{\sigma_k}\frac{\partial k}{\partial x_i}\right) + \rho P - \rho\varepsilon \tag{4.18}$$

and

$$\frac{\partial(\rho \varepsilon)}{\partial t} + \frac{\partial(\rho \bar{u}_i \varepsilon)}{\partial x_i} = \frac{\partial}{\partial x_i}\left(\frac{\mu_t}{\sigma_\varepsilon}\frac{\partial \varepsilon}{\partial x_i}\right) + C_1 \rho P \frac{\varepsilon}{k} - C_2 \rho \frac{\varepsilon^2}{k}, \tag{4.19}$$

where P is production of turbulence by shear in the mean flow, introduced in Sec. 4.3.5

Maele & Merci (2006) specify that the term *standard* is used when the turbulence viscosity, ν_t, is calculated by using of k and ε. Tennekes & Lumley (1972, p. 11) show that the eddy viscosity, ν_t, can be expressed in terms of characteristic length and velocity scales in the turbulence, $\nu_t \sim u'l'$. While the k-ε model actually filters out the varying length scales (see Fig. 6.7, p. 52), an integral length scale can be expressed as $l' \sim k^{3/2}/\varepsilon$. The characteristic velocity of the turbulent fluctuations is $u' \sim k^{1/2}$, resulting in the standard

$$\nu_t = C_\mu \frac{k^2}{\varepsilon}. \tag{4.20}$$

For these equations, Launder & Spalding (1974) chose the model constants that are know considered *standard*. These are listed in Table. 4.1.

Table 4.1: The model constants used in the simulations

C_μ	C_1	C_2	σ_k	σ_ε
0.09	1.44	1.92	1.0	1.3

Some alterations introduced in Ch. 7 are done with the sole intent of adjusting these constants to better describe the atmospheric boundary layer flow. Nevertheless, the values in Table 4.1 are what can be considered the accepted standard.

4.3.3 The law of the wall

In a standard k-ε model, wall effects are included with laws of the wall.

A dimensionless velocity and length scale for use in close proximity to solid boundaries can be expressed as

$$u_1^+ = \frac{\bar{u}_1}{u_*} \qquad \text{and} \qquad x_2^+ = \frac{x_2 u_*}{\nu}. \tag{4.21}$$

Ertesvåg (2000, pp. 70–77) discusses how how the flow in the area $x_2^+ < 100$ is defined by much intermittency. There are large gradients for several mean values, which results in a substantial production of turbulence. It is therefore safe to assume that how this area of the flow is modeled, has a large impact on the results.

As the distance to the wall tends to zero, the molecular transport is dominant in the flow. This *viscous* or *laminar sublayer* is often restricted to the region where $x_2^+ < 10$. The velocity in this region reduces down to

$$u_1^+ = x_2^+. \tag{4.22}$$

Outside this laminar sublayer, turbulence related transport is relevant, and the flow is in the *logarithmic sublayer*. Consider an analogy to the large-scale flow of planetary boundary layer, where the *surface layer* (see Sec. 3.2.2) is defined as a region where the momentum and heat fluxes are constant. The velocities in *this* logarithmic sublayer is assumed to be distributed across a logarithmic profile. This is based on measurements showing that the velocity gradient is

$$\frac{d\bar{u}_1}{dx_2} = \frac{u_*}{\kappa x_2}. \tag{4.23}$$

An additional assumption of small gradients for the convective and diffusive transport of turbulence kinetic energy (i.e. balance between production and dissipation of k), gives the following laws of the wall:

$$u_1^+ = \frac{1}{\kappa} \ln(E x_2^+) \tag{4.24}$$

$$\varepsilon = \frac{u_*^3}{\kappa x_2} \tag{4.25}$$

$$k = \frac{u_*^2}{\sqrt{C_\mu}} \tag{4.26}$$

4.3.4 Low Reynolds number k-ε model

While the k-ε model presented in the previous sections gives a complete closure of a flow problem, there are other approaches to account for laminarization effects where μ_t and μ are of comparable magnitude.

Jones & Launder (1972) suggested one such approach. By adding one term to both transport equations, and including new low Reynolds number factors, these

new relations are

$$\frac{\partial(\rho k)}{\partial t} + \frac{\partial(\rho \bar{u}_i k)}{\partial x_i} = \frac{\partial}{\partial x_i}\left(\left(\mu + \frac{\mu_t}{\sigma_k}\right)\frac{\partial k}{\partial x_i}\right) + \rho P - \rho\varepsilon - 2\mu\left(\frac{\partial k^{1/2}}{\partial x_j}\right)^2 \tag{4.27}$$

and

$$\begin{aligned}\frac{\partial(\rho\varepsilon)}{\partial t} + \frac{\partial(\rho\bar{u}_i\varepsilon)}{\partial x_i} =& \frac{\partial}{\partial x_i}\left(\left(\mu + \frac{\mu_t}{\sigma_\varepsilon}\right)\frac{\partial \varepsilon}{\partial x_i}\right) + \\ & C_1 f_1 \rho P\frac{\varepsilon}{k} - C_2 f_2 \rho\frac{\varepsilon^2}{k} - 2.0\nu\mu_t\left(\frac{\partial^2 \tilde{u}_i}{\partial x_j x_l}\right)^2.\end{aligned} \tag{4.28}$$

where there has also been factored in a low-Reynolds number effect in the turbulence related viscosity,

$$\nu_t = C_\mu f_\mu \frac{k^2}{\varepsilon}. \tag{4.29}$$

The three new factors have the forms

$$f_1 = 1.0, \tag{4.30}$$

$$f_2 = 1.0 - 0.3\exp\left(-\mathrm{Re}_t^2\right), \tag{4.31}$$

and

$$f_\mu = \exp\left(\frac{-2.5}{1 + \mathrm{Re}_t/50}\right), \tag{4.32}$$

where the local turbulence Reynolds number is defined

$$\mathrm{Re}_t = \frac{k^2}{\nu\varepsilon}. \tag{4.33}$$

4.3.5 Production terms

There are two production terms in Eq. (4.43), production of turbulence by shear stresses, P, and production by buoyancy forces, G.

P is calculated as

$$\rho P = \mu_t\left(\frac{\partial \bar{u}_i}{\partial x_j} + \frac{\partial \bar{u}_j}{\partial x_i}\right)\frac{\partial \bar{u}_i}{\partial x_j} - \frac{2}{3}\left(\rho k + \mu_t\frac{\partial \bar{u}_l}{\partial x_l}\right)\frac{\partial \bar{u}_i}{\partial x_i}, \tag{4.34}$$

where the normal stresses are often neglected in situations with small density variations (Ertesvåg, 2000, p. 55).

To account for turbulence production or dissipation due to buoyancy effects, the Boussinesq approach can be used (Ertesvåg, 2000, p. 57)

$$G = \alpha(-\overline{u_i' T'})f_i, \tag{4.35}$$

where α is the volumetric expansion coefficient, T is the temperature and f_i is the gravitational acceleration in the x_i direction. This expression can further be

modeled with a gradient model as

$$G = \alpha \frac{\nu_t}{\sigma_{T,t}} \frac{\partial \overline{T}}{\partial x_i} f_i, \tag{4.36}$$

using $\sigma_{T,t}$ as a turbulence Prandtl number. The typical relation $\nu = \mu/\rho$ is valid also for turbulence related viscosity.

The effect of G is not included in the transport equations listed so far. This can be directly applied in either transport equation for k, Eqs. (4.18) and (4.27), while Patel *et al.* (1985) state that using a constant C_3 that depends on the stability should be included when using $(\varepsilon/k)G$ in the equations for ε, Eqs. (4.19) and (4.28).

4.3.6 The implementation in KFX

The last sections has shown two versions of the k-ε model, where the one listed as a high-Reynolds number model often referred to as the *standard*. While the production term from buoyancy effects, G, can be included to account for slight temperature gradients.

To include the effect of density variations, the momentum, k and ε equations should use Favre averaged quantities, as is done in KFX. Except for the previous sections, k and ε respond to their Favre averaged values in the rest of this thesis.

Using Favre averaged quantities, k and ε are defined

$$k = \frac{1}{2} \widetilde{u_i'' u_i''} \tag{4.37}$$

and

$$\varepsilon = \nu \widetilde{\left(\frac{\partial u_i''}{\partial x_j} \right)^2}. \tag{4.38}$$

Note that the averaging is done for the whole, squared expression in Eq. (4.38).

The Reynolds stresses and production due to shear in the mean flow now include effects of the possible divergence in the flow field

$$-\bar{\rho} \widetilde{u_i'' u_i''} = \mu_t \left(\frac{\partial \widetilde{u_j}}{\partial x_i} + \frac{\partial \widetilde{u_i}}{\partial x_j} \right) - \frac{2}{3} \left(\bar{\rho} k + \mu_t \frac{\partial \widetilde{u_l}}{\partial x_l} \right) \delta_{ij} \tag{4.39}$$

and

$$\bar{\rho} P = \mu_t \left(\frac{\partial \tilde{u}_i}{\partial x_j} + \frac{\partial \tilde{u}_j}{\partial x_i} \right) \frac{\partial \tilde{u}_j}{\partial x_i} - \frac{2}{3} \left(\bar{\rho} k + \mu_t \frac{\partial \tilde{u}_l}{\partial x_l} \right) \frac{\partial \tilde{u}_i}{\partial x_i}, \tag{4.40}$$

While the gravitational acceleration is no longer explicitly present in the exact transport equation for k (Ertesvåg, 2000, Eq. (B.42)), turbulence production by buoyancy is included in KFX through a production term G, which is now expressed through density variations,

$$G = \bar{\rho} \widetilde{u_i'' \rho''} f_i, \tag{4.41}$$

Then, a standard gradient model is applied to get the expression

$$G = -\frac{\mu_t}{\sigma_{T,t}} f_i \frac{\partial \bar{\rho}}{\partial x_i}, \tag{4.42}$$

where $\sigma_{T,t} = 0.7$.

KFX currently utilizes approaches from both the high- and low-Reynolds number models outlined Secs. 4.3.2 and 4.3.4. This may have some unfortunate effects, as will be discussed in the next section.

All in all, the transport equation for k used in the simulations in this thesis is then expressed

$$\frac{\partial \bar{\rho} k}{\partial t} + \frac{\partial (\bar{\rho} \tilde{u}_i k)}{\partial x_i} = \frac{\partial}{\partial x_i} \left(\left(\mu + \frac{\mu_t}{\sigma_k} \right) \frac{\partial k}{\partial x_i} \right) + \bar{\rho} P - \bar{\rho} \varepsilon + G. \tag{4.43}$$

And similarly, including some of the low-Reynolds number effects, the transport equation for ε is

$$\frac{\partial \bar{\rho} \varepsilon}{\partial t} + \frac{\partial (\bar{\rho} \tilde{u}_i \varepsilon)}{\partial x_i} = \frac{\partial}{\partial x_i} \left(\left(\mu + \frac{\mu_t}{\sigma_\varepsilon} \right) \frac{\partial \varepsilon}{\partial x_i} \right) + C_1 f_1 \bar{\rho} P \frac{\varepsilon}{k} - C_2 f_2 \bar{\rho} \frac{\varepsilon^2}{k} + C_1 C_3 \frac{\varepsilon}{k} G, \tag{4.44}$$

where the rightmost terms from Eqs. (4.27) and (4.28) are excluded. C_3 takes the values of 1 or 0 depending on whether the local stability is unstable or stable, respectively (Patel *et al.*, 1985).

These equations are in KFX used together with the laws of the wall, described in Sec. 4.3.3. It is shown in Sec. 7.4.7 that this treatment of the boundaries is not a substantial source of errors in large scale modeling with KFX.

4.3.7 Idiosyncrasies

Any code developed over longer periods of time, will contain characteristics that intentionally and unintentionally separates it from the alternatives, and KFX is no exception. Especially the low-Reynolds number effect, which are in use in the calculations done here, are a topic for debate. Patel *et al.* (1985) did a review of the then current state of low-Reynolds number modifications to the k-ε model. A number of different models were tested, but a common factor was that no model had both low-Reynolds number modifications and laws of the wall in use. This is because the modifications are meant to improve the wall effect, since the main area with low Reynolds numbers is close to the walls.

Hopefully, this indicates that the modifications in KFX are overruled by the laws of the wall in most cases. This was not discovered until the end of the work on this thesis, so only a simple test of this hypothesis was practical. Figure 4.1 shows the effect disabling these terms had on the simulation results for the Thorney Island scenario (see Sec. 6.1.1 for description). The differences that occur when using the low-Reynolds number effects in KFX are noticeable, but seem small enough to neglect their contribution to the results in the rest of the thesis.

Most likely there are more such sources of uncertainty that will remain undis-

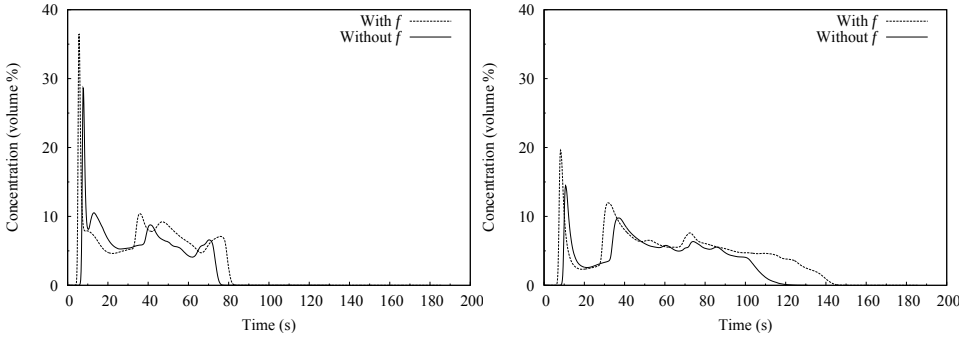

(a) Measuring point 1 (b) Measuring point 2

Figure 4.1: The effect of disabling the low-Reynolds number effects

covered. The models described in this chapter are, nevertheless, what is used in KFX, unless otherwise stated. This software has shown favorable comparisons with experimental data over the course of years, but it is the right for any user to stay critical to the results.

4.3.8 Applicability to dense gas dispersion in an ABL

Ertesvåg (2000, pp. 60-61) comments on some areas the k-ε model has troubles describing correctly. Three of these effects are often present in a typical simulation of a dense gas release. The first is strong curvature in the flow, as in wakes behind fences; the second is a strong anisotropy (orientation dependency) in the Reynolds stresses, here due the stratification in the dense gas; and finally the directionally varying forces from buoyancy effects, which are attempted to account for by using Favre averaging.

That being said, even higher order closures, such as solving transport equations for each Reynolds stress, do not completely remove these trouble area.

The models up to, not including, LES have also a common problem with length scales. The equations will lead to one scalar (i.e. not directed) length scale ($l' \sim k^{3/2}/\varepsilon$, in the k-ε model) that is meant to represent all sizes of eddies. In a high-intensity turbulent flow, say a jet flame, in an otherwise turbulent atmosphere, this is bound to be a source of errors, as determining the constants is to a degree dependent on the scenario.

It has been shown that the standard model constants listed in Table 4.1 tend to underestimate the dissipation rate of ε, resulting in an overestimation of k downstream in the domain (Freedman & Jacobson, 2003). Other alterations to the k-ε model are studied in Ch. 7.

5 CFD software

As stated in Sec. 4.1.1, simpler models than the fully three-dimensional RANS-models soon become insufficient if gas releases are to be modeled accurately. Computational fluid dynamics (CFD) is an umbrella-term for the process of solving the new transport equations present in such models, and it is also often used for the related software.

5.1 General CFD and KFX

Versteeg & Malalasekera (2007, pp. 2–8) explain how most CFD packages are structured, which involves three main elements. These three elements are a pre-processor, a solver and a post-processor. This section provides a brief description of these, while relating them to their KFX counterparts.

5.1.1 Background

There are a well of different CFD software packages, and their intended use may vary substantially. Multiphase flow in pipes is a typical computational problem in the process industry, and CFD codes aimed at solving this are completely different from those directed at an aerodynamics engineer's study of flow over airfoils. How general a software is will be a trade-off between scope of use and accuracy in each area. The more general a code is, the less accuracy can be expected in the different scenarios.

Kameleon FireEx (KFX) is a flow and fire simulator now developed by Computational Industry Technologies AS (ComputIT) and has been since 1999. KFX is a complete CFD software package, where the problem is defined and solved and the results can be presented graphically. KFX is based on a three-dimensional combustion code that a research team at SINTEF Energy Research and NTH had running as early as in the 1970s (Danielsen, 2000), and its main use is still in combustion problems.

5.1.2 Pre-processor

The pre-processing stage of a CFD simulation is the area where the user gives input to the code. Versteeg & Malalasekera (2007) describe several steps involved in this stage: defining the geometry; generating the grid; selecting the physical models; defining fluid properties; and specifying appropriate boundary cells.

Defining the geometry and generating the grid are the most time-consuming aspects of a CFD simulation, according to Versteeg & Malalasekera (2007) this take 50% of the time spent on CFD. Most CFD software now have the ability to import three dimensional models from CAD (computer-aided design) software, making it is easier to get a realistic representation of the calculation domain than it would be if the cells had to be defined manually. How the grid, or mesh, is set up has a huge impact on the results the software delivers, and with today's software it is still up to the user to define a grid that is suited for the task at hand. This puts a demand on the user to have an understanding of how the flow will develop, so that the mesh can be defined finer in areas with steep gradients.

Most commercial CFD software (including KFX) has an extensive selection of fluid properties. This means that the chosen physical models (e.g. turbulence and combustion models) can have input parameters which are as accurate as possible.

KFX uses a graphical user interface (GUI), which is arguably the most common way of doing it, the alternative being an entirely command-based user interface. In KFX, this GUI is called Lizard.

5.1.3 Solver

KFX uses the finite volume method (FVM) to solve the partial differential equations describing the behavior of fluids. In this method, conservation of flow variables is ensured by going through three main steps: integrating the governing equations over the finite control volumes; discretizing the resulting integral equations; and finally solving these algebraic equations by an iterative method (Patankar, 1980). This can be expressed by a verbal version of Eq. (4.6) (Versteeg & Malalasekera, 2007, p. 4):

$$\begin{bmatrix}\text{Rate of change of } \phi \text{ in the control volume with respect to time}\end{bmatrix} = \begin{bmatrix}\text{Net rate of increase of } \phi \text{ due to convection into the control volume}\end{bmatrix} + \begin{bmatrix}\text{Net rate of increase of } \phi \text{ due to diffusion into the control volume}\end{bmatrix} + \begin{bmatrix}\text{Net rate of creation of } \phi \text{ inside the control volume}\end{bmatrix}$$

KFX's solver, Kameleon, uses a solution algorithm called SIMPLEC, which is a pressure-correction linkage between the continuity and momentum equations. These equations are solved with a TDMA (tri-diagonal matrix algorithm) scheme, or via a version of the Stone algorithm (Stone, 1968).

5.1.4 Post-processor

After the solver has gone through all its iterations and the results are gathered, most software packages has means of presenting these results graphically. This is often done by presenting the results as iso-contours or vector fields in cross-sections of the three dimensional geometry.

KFX also gives the user the opportunity to view the results as they are calculated. While the term *post-processing* is not strictly appropriate for this, it is still

done in a similar manner.

Even if the solver portion is by far the most computer demanding, the user will spend most time in the pre- or post-processing stages. As CFD software become more and more used, developers spend an increasing portion of their time on these two areas.

5.1.5 Solution procedure SIMPLEC

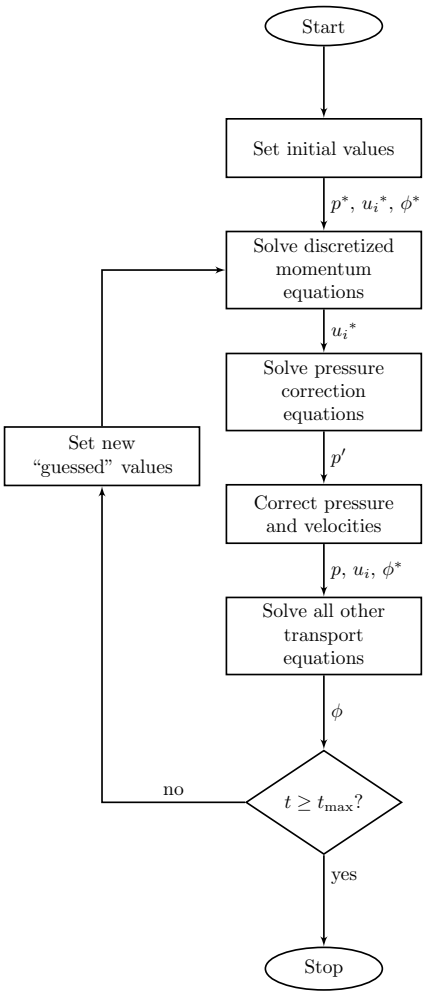

Figure 5.1: Flowchart

The SIMPLEC algorithm is an improved version of the standard SIMPLE procedure. Some terms are neglected in both algorithms, the difference being that of the two, SIMPLEC neglects the least significant terms.

The procedure for a transient simulation is shown in Fig. 5.1, which is an adaptation from Fig. 6.6 in Versteeg & Malalasekera's (2007) book.

KFX sets the initial values in the entire domain, depending on what wind parameters and other flow parameters the user has defined. These values are then used as an initial "guess" entering the procedure (values marked with an asterisk in Fig. 5.1).

These values are used in discretized versions of the momentum equations (Eq. (4.13)). The resulting velocities are then used to solve a pressure correction equation, which is based on the continuity equation. In a FVM method, where conservation of variables is both a strength and an important factor, such a term must be calculated with a high degree of accuracy.

The corrected pressure is then used to find new values for the pressure and velocities, before the transport equations for other flow variables, such as k, ε and $\widetilde{Y}_l$, are solved. The program then checks the new time and it continues if a termination criteria has not been reached.

Notice that the version of SIMPLEC used in KFX does not check for convergence in each time step. Versteeg & Malalasekera (2007) suggest using an inner convergence criteria before controlling

if the termination criteria has been reached. In KFX it has been opted to use relatively small time steps to ensure a non-diverging solution. There are still spent considerable resources on iterative processes, as convergence is still needed in each calculation step, especially in the pressure corrections equations. These are solved with a Stone algorithm, which is a strongly implicit, iterative procedure (Stone, 1968). The other steps are handled by traditional TDMA solvers.

5.2 Numerical scheme

The equations presented in this section show how the physical models are discretized and organized before the solver in KFX handles them. The equations are based on information given by Vembe *et al.* (2010), but they are by no means exclusive to KFX. There are many other sources to such information, and similar schematics are used in several CFD software packages.

5.2.1 The grid

If all flow variables are calculated at the same points, some characteristic problems arise (Patankar, 1980; Versteeg & Malalasekera, 2007). One such problem is how a momentum equation used with a linear interpolation scheme to find the surface values, will have no problem with a pressure field with alternating high and low values. It will *feel* this checkerboard pressure field as if it was uniform.

One way to avoid this problem is to calculate some key flow variables in a different grid. The typical procedure for this, and the one used in KFX, is having a *staggered grid*. A two dimensional version of this is shown in Fig. 5.2, which is adapted from Patankar (1980, Fig. (6.6)).

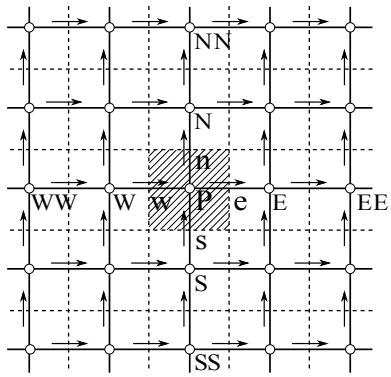

Figure 5.2: Nodes for scalars and u and v, staggered grid

In Fig. 5.2 the nodes in the neighboring cells of the P-node cell are noted with capital letters, corresponding to the cardinal points, and the cell surfaces are noted with small letters. For a three-dimensional setup, as is used in most industrial applications, a bottom layer (B) and a top layer (T) would be added. This three-dimensional approach is used in KFX.

5.2.2 Boundary conditions

The transport equations for scalars and momentum are not solved for cells immediately adjacent to walls, where boundary functions or laws of the wall are used.

In Sec. 4.3.3 the laws of the wall for the scalars k and ε were introduced. In numerical calculations, how one treats solid boundaries are one of the main challenges. If the laws of the wall are used to find the scalar values in nodes adjacent to walls, one of several cases may occur. The position of the node, y^{p}, might be inside the laminar sublayer. Here, the laws of the wall used in KFX are found by expressing the dimensionless distance as $y^+ = \sqrt{u_p y_p/\nu_p}$, which gives a frictional velocity of (Vembe *et al.*, 2010)

$$u_* = \sqrt{\frac{\tau_w}{\rho_p}} = \sqrt{\frac{\nu_p u_p}{y_p}}) = \frac{u_p}{y^+}, \tag{5.1}$$

which is used to find k and ε through

$$k_p = \frac{u_*^2}{\sqrt{C_\mu}} \left(\frac{u_p}{u_* y^+_{edge}} \right)^2, \tag{5.2}$$

and

$$\varepsilon_p = \frac{u_*^4}{\kappa \nu_p y^+_{edge}}, \tag{5.3}$$

where $y^+_{edge} = 10.5$. The laminar, or viscous sublayer ordinarily corresponds to very small values of y^{p}, meaning that it is seldom used.

If, however, the value of y^{p} gives a value of y^+ that is in the logarithmic layer (i.e. $10 < y^+ < 1000$), the values in y^{p} are set to those given by Eqs. (4.26) and (4.25). This is also used even if y^{p} is placed outside the log-law regime (i.e. $y^+ > 1000$), as the profile in an area outside the logarithmic region often is fairly logarithmically shaped (Vembe *et al.*, 2010).

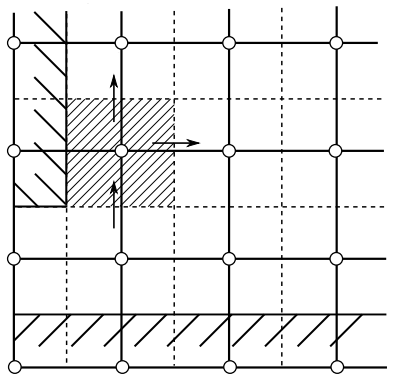

Figure 5.3: Nodes for scalars and u and v, staggered grid

Figure 5.3 shows a situation where the node of interest adjacent to a solid boundary. When these nodes are solved in KFX, the values for k and ε are numerically frozen. This means that the nodes adjacent to solid walls are treated as boundary conditions for the surrounding flow. To get these values as accurate as possible, it is important to have a fine grid close to the wall.

5.2.3 Solving transport equations

While this section might initially seem a bit elaborate, all is included here to better explain how some modifications were added in Sec. 7.4.

Starting with a transport equations for a scalar variable,Eq. (4.6), after discretization this can be expressed as

$$\frac{(\rho\phi - \rho^0\phi^0)}{\Delta t}\Delta V + J_e - J_w + J_n - J_s + J_t - S_\phi \Delta V = 0 \tag{5.4}$$

after discretizing and integrating over a cell's volume (finite volume method). Here the superscript 0 denotes values from the previous time step, Δt is the length of the current time step and S_ϕ is the source term. J_j indicates total flux through control surface j, and is defined as

$$J_{x_i} = \left(\rho u_i \phi - \Gamma \frac{\partial \phi}{\partial x_i}\right) \Delta A_{x_i}, \tag{5.5}$$

where ΔA_{x_i} is the control surface area. If the continuity equation is discretized in a similar manner, the result is

$$\frac{(\rho - \rho^0)}{\Delta t}\Delta V + F_e - F_w + F_m - F_s + F_t - F_b = 0, \tag{5.6}$$

where F_j is the total mass flux through control surface j, expressed as

$$F_{x_i} = \rho u_i \Delta A_{x_i}. \tag{5.7}$$

Now, if Eq. (5.6) is multiplied by ϕ_p and subtracted from Eq. (5.4) (Vembe *et al.*, 2010, Eq. (5.6)) is obtained.

$$\begin{aligned}(\phi - \phi^0)_p \rho_p^0 \frac{\Delta V}{\Delta t} &+ (J_e - F_e\phi_p) - (J_w - F_w\phi_p) \\ &+ (J_n - F_n\phi_p) - (J_s - F_s\phi_p) \\ &+ (J_t - F_t\phi_p) - (J_b - F_b\phi_p) - S\Delta V = 0.\end{aligned} \tag{5.8}$$

Equation (5.8) includes vectors, u_i, which are unknown and located on the control volume surface. If a first-order approximation scheme (Patankar, 1980) is used, a term $(J_j - F_j\phi_p)$ is expressed

$$(J_j - F_j\phi_p) = a_J(\phi_p - \phi_J)(-1)^d, \tag{5.9}$$

where d equals 0 for positive directions ($j = e, n, t$, $J = E, N, T$) and 1 for negative directions ($j = w, s, b$, $J = W, S, B$). Now each coefficient a_J may be expressed

$$a_J = \left(\frac{\Gamma_j \Delta A_{x_i}}{\delta x_j} \right) + (\max((-1)^{(d+1)} F_j, 0), \tag{5.10}$$

where i is 1 for the x-direction, 2 for the y-direction and 3 for z-direction, and δx_j is the distance between the two grid nodes separated by the j surface.

In KFX it is used a second order upwind (SOU) scheme. The upwind schemes were developed to overcome a shortcoming of central differencing schemes, that "the convected property ϕ_e at the interface is the average of ϕ_E and ϕ_p" (Patankar, 1980, p. 83), and for a first-order approximation it can be written out

$$\phi_w = \phi_W \qquad \text{if} \qquad F_w > 0, \tag{5.11a}$$

and

$$\phi_w = \phi_p \qquad \text{if} \qquad F_w < 0. \tag{5.11b}$$

Equation (5.11) show the upwind scheme for a first-order discretization. As mentioned, KFX uses a second-order type of this scheme. For the corresponding case with $F_w > 0$, the SOU would give

$$\phi_w = \phi_W + \frac{\delta x_W}{\delta x_W + \delta x_{WW}} (\phi_W - \phi_{WW}). \tag{5.12}$$

Only the source term S_ϕ is left unknown in Eq. (5.4). This source can safely be assumed to be a function of the scalar (i.e. $S_\phi = S_\phi(\phi)$) and needs to be treated before it is solved numerically. A typical way of doing this, is to do a first order Taylor expansion, or what in effect is a linearization. The resulting source then consists of a constant (i.e. not dependent on the current time step) and a proportional part. Using S_C as the constant part and S_P as the proportional term, the source becomes

$$S = S_C + S_P \phi_p. \tag{5.13}$$

Going through this entire procedure leaves a system of linear equations (i.e. $A\phi = b$) which for each node is summed up as

$$a_p \phi_p = \sum a_{\text{nb}} \phi_{\text{nb}} + b, \tag{5.14}$$

where nb indicates neighbour node.

The center-point coefficient is then given by

$$a_p = a_E + a_W + a_N + a_S + a_T + a_B + \frac{\rho^0 \Delta V}{\Delta t} - S_P \Delta V \tag{5.15}$$

and the constant b is calculated as

$$b = b_{\text{sou}} + S_C \Delta V + \phi_p^0 \frac{\rho^0 \Delta V}{\Delta t}, \tag{5.16}$$

where b_{sou} contains the contribution from the neighbours' neighbour effect occurring when using a second order upwind scheme.

After this procedure is gone through for all grid cells and transport equations, the software is ready for the next time step—rinse and repeat.

6 The test scenarios and initial KFX results

This chapter has a twofold focus—describing both of the test cases used in the simulations and provide an initial assessment of the results from these.

6.1 The scenarios used in KFX

The current version of KFX is tested with two scenarios. The aim of the first is to study the k-ε model's handling of near field dense gas flow, a scenario based on trial 21 of the Thorney Island dense gas releases, and the second's aim is to see how it copes with the far field atmospheric boundary layer.

6.1.1 Thorney Island

The Thorney Island dense gas release trials were conducted in the early 1980s. These were a set of trials divided into three phases, each designed to show some specific characteristic of a dense gas release. The Phase I trials were done to see how an undisturbed, instantaneous release of dense gas behaved; the Phase II trials included obstacles in an instantaneous release; while the Phase III trials were of an undisturbed continuous release (McQuaid & Roebuck, 1985).

Comparisons between KFX and Thorney Island data (all of which are collected from Andronopoulos *et al.* [1994]) are meant to show how KFX and the alterations to KFX treat near field dense gas effects.

The work for the specialization project was with one specific trial, trial 21, from the Phase II releases. In that trial, a 2050 m^3 cylinder of gas with an initial relative density, $\rho_r = \rho/\rho_a$, of 2.02 was instantaneously released into a neutral atmosphere with a wind speed of 3.9 m/s. Surrounding the cylinder, at a radial distance of 50 m, was an impenetrable, 5 m tall fence. One of the main reasons for using a trial from these experiments is that the gas was isothermal and non-reacting, making it possible to adequately isolate the flow phenomena specific for dense gas releases.

Figure 6.1 shows a sketch of the test area, with the release cylinder and the 5 m tall, semi-circular fence, which surrounds the release point with a radial distance of 50 m. From this, most of the data comparison here will be with the first two measuring points (MP1 and MP2), both at a height of 0.4 m. These were chosen since their results seemed representable for KFX's current handling of dense gas, to amplify any three-dimensional effects, and being on the upwind side of the fence.

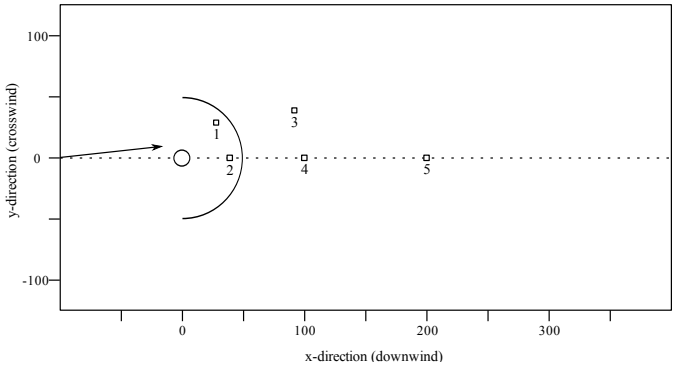

Figure 6.1: A sketch of the test area for Thorney Island trial 21

6.1.2 Empty wind field

The second test case' objective is to show as isolated as possible how KFX copes with the surrounding wind, especially far down-stream in a large domain. This part is not compared to experimental data directly, but assuming a wanted laterally homogeneous flow field, the most obvious comparison is between the domain values and the upwind boundary itself.

An argument can be made on that the results from this scenario is greatly determined by the upwind boundary. As stated in Sec. 3.3, there is no conclusive way to express these boundaries, and the empirical data vary to some degree. The assumption made here is then that a consistent expression of k and ε would not represent a physically realistic setup of these values. It is therefore reasonable to say that this will be a test of the actual model's performance, rather than a check of the validity of the boundaries.

Whereas the simulations done with Thorney Island trial 21 are highly transient, since the release is instantaneous, these wind calculations are run over a period sufficiently long to remove any time derivatives. This is ensured by running the simulations for longer than it takes the mean wind of 5 m/s to travel through the whole domain.

The results from these tests are presented in graphs showing the initial boundary with its actual values as a drawn line, while dashed lines represent the developed deviations at 400 m or 900 m downstream.The symbol $\Delta_{\%}\phi$ is used to express a deviation of a flow variable ϕ in percents of the boundary value.

6.2 Grid dependence

Versteeg & Malalasekera (2007, p. 5) say that "the only way to eliminate errors due to coarseness of a grid is to perform a grid dependence study." A grid dependence study is then described as starting with a coarse grid, and then refining it progressively until key results do not change. In addition to a typical grid dependence study there is done a test to see how the total domain height influence the results in the empty domain.

6.2.1 Thorney Island

Figure 6.2 shows the calculated results from the initial KFX simulation, and two additional simulation results. In these simulations there are used finer grids than in the simulation in the specialization project, and by only changing the grid refinement, the influence from the grid is isolated. In a dense gas release simulation, there are large gradients in the vertical direction, while the lateral variations are much smaller. The results presented here are therefore done with a grid first refined in the z-direction, then in the lateral directions around the release point.

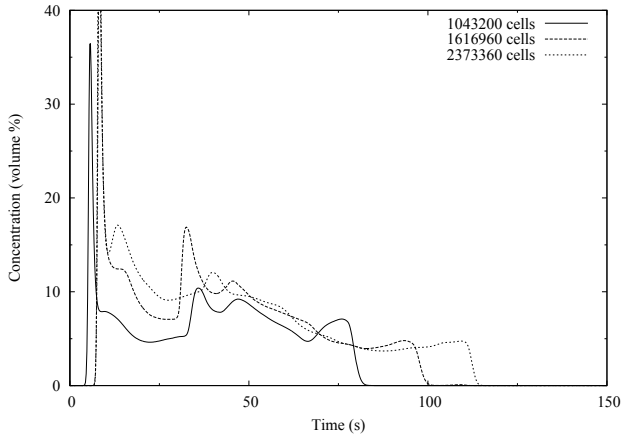

Figure 6.2: Grid dependence of Thorney Island results

These results are not interesting in and of themselves, as it would be necessary to do further analysis to reach the point where the concentration development stays independent of grid-refinement. They are, nonetheless, evidence of the influence of the grid on the results, even at these fairly high cell-counts. It is worth noting that the study by Andronopoulos *et al.* (1994) of the Adrea-HF code on the same test-case was done with 27508 cells for a similar domain size. That model achieved results of quality comparable to the KFX results presented here, which shows how a simpler model, dedicated to one task can excel in that area.

Even with the finest grid the gas is lifted too soon over the fence, and it is unlikely that this effect is due to the grid alone. Either way, it is not beneficial if the grid has to be refined to a unpractical resolution, for a model to give satisfying results.

Depending on when the actual simulations took place, it may have been used both the finest and coarsest grids in the results presented here. Figure 6.2 shows similar trends for all three simulations, and results from any alterations should be equally scalable. When simulation results are compared, identical scenarios are used between the simulations.

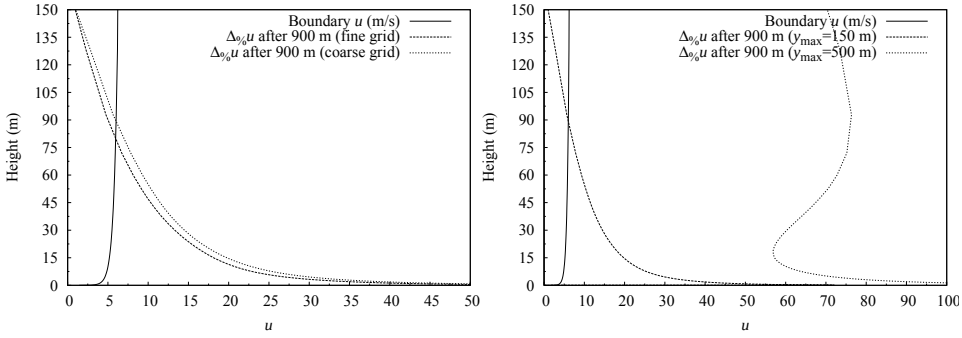

(a) Grid dependence (b) Domain height

Figure 6.3: Domain configurations of empty wind domain

6.2.2 Empty wind field

The empty wind field scenario, which had a base area of 100 m by 1 km, was tested for grid dependency by having cells with base area of either 1 m^2 or 4 m^2 uniformly distributed. Figure 6.3a shows how changing the base area of the cells had insignificant impact on the downwind results. Thus, to minimize computational time, the coarsest setup was used on the rest of the simulations. The vertical distribution of cells was kept constant, with a fine grid close to the surface, parabolically increasing upwards. The cells closes to the surface had a height of 0.2 m, to ensure that the steep gradients where represented, while the uppermost cells were 44 m tall.

It was also wanted to do a study of the total domain height, the thought being the results in the lower 150 m should remain unaltered even if the *total* domain height is changed from 150 m to 500 m. The upper boundary condition should then have little or no impact on the results. Keep in mind that the used version of Monin-Obukhov's theory is only meant for a height of 10% of the atmospheric boundary layer height. A total domain of 500 m is therefore probably outside the valid range of the similarity theory. Only the lower 150 m in either case are considered here.

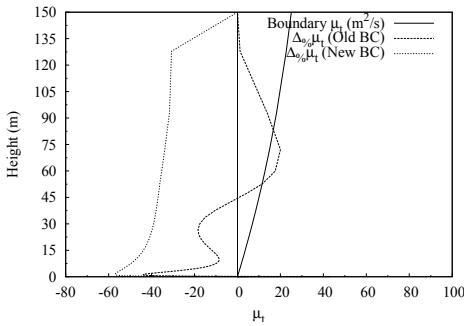

Figure 6.4: The effect of the boundary conditions on μ_t (after 900 m)

The results of this study of the domain height, shown in Fig. 6.3b, are not as encouraging as those for the grid refinement. The deviation from the boundary value seems to explode as the total domain height increases, a peculiarity that proved to be due to a forgotten feature in the KFX code. In a comprehensive code such as KFX, there are bound to be some long-forgotten lines that were meant to be deleted.

As is shown in Fig. 6.4, effects of

the upper boundary condition propagate through the entire height of the domain. The first dashed line, which shows the deviation 900 m downstream with the old, erroneous boundary condition, has a completely different shape than the uniformly negative one of the second dashed line. Since this was an unintentionally left-over artifact in the code, it does not relate directly to a part of KFX in need of improvement, but it is nevertheless a reminder of how small alterations can have a significant impact on results, a point well-worth remembering when new alterations to the code are tested in the next chapter.

6.3 Wind profile parameters

The wind profile used in the specialization project work had a roughness height of $z_0 = 0.0002$m, which is the standard for open sea (Huser *et al.*, 1997). McQuaid & Roebuck (1985) note that there was a substantial grass height on the test field used for the Thorney Island trials. How do changing this roughness height affect the calculation results?

6.3.1 Thorney Island

The scaling roughness height, z_0 in Eq. (3.9), from Monin-Obukhov's similarity theory is a characteristic surface roughness height. Altering this changes the surface friction tension, τ_0, thus also the wind's friction velocity, u_*.

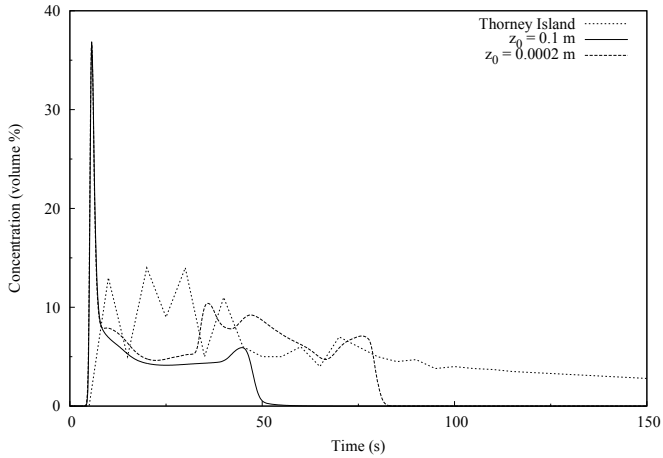

Figure 6.5: The effect of changing the scaling roughness height, z_0. Measuring point 1, Fig. 6.1

While the results shown in Fig. 6.5 seem to have a smaller deviation than those present in Fig. 6.2, changing z_0 alters the characteristics of the concentration curve, but gives the same abrupt "stop" as previously. Increasing the aerodynamic roughness does therefore not improve the gas' tendency to disperse too quick over the fence.

The reason for this is that the increased turbulence in the wind tends to dilute the lower concentrations more, and also spreading the gas more close to the ground on the upwind side of the fence.

The setting of the wind model parameters that was used for the initial results were tentative, at best. With both more time and better experimental measurements, the simulation results could be of a much closer fit to the experimental data.

6.3.2 Empty wind field

KFX uses an implementation of the Monin-Obukhov theory that is only valid for stable and neutral atmospheric conditions (see. Sec. 3.3). The typical stability parameter, $\zeta = z/L$, has the limits of $\zeta \to 0$ for a neutral and $\zeta \to \infty$ for a stable atmosphere. These limits are tested here with two values of L, the Obukhov length, for a neutral atmosphere, $L = 10000$ and for a stable atmosphere $L = 360$. KFX's initial handling of these two settings is shown in Fig. 6.6.

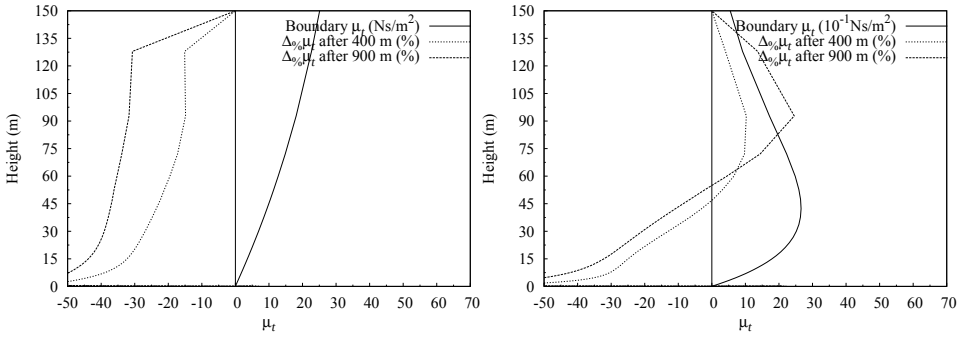

(a) $L = 10000$m (b) $L = 360$m

Figure 6.6: Visualization of the unpredictability of turbulence development between stability regions

The most prominent feature of these results is, aside from the fairly large deviations in both, the seeming unpredictability between the stability configurations. In the neutral case, Fig. 6.6a, a steady declination of the turbulence related viscosity is shown. For the stable stratification, however, the deviation is similar to that in the neutral scenario in the lower portions, but as $\partial\mu_t/\partial x_3 < 0$ the deviation turns positive—the turbulence related viscosity *increases* downstream.

In the neutral case, k is practically independent of x_3, which means that it is safer to assume local equilibrium (see App. A), whereas $h \gg 150$ is no longer valid for a stably stratified flow, and k varies substantially with the height. It will therefore be difficult to merely recalibrate the model constants to achieve a homogeneous solution, while still keeping the generality of even the wind modeling. Any approaches to alterations that aim to be valid over the entire range must then

either be a) using turbulence dependent functions for one or more model constants, or b) an additional term in the turbulence model.

6.4 Comments

This section provides comments on the results obtained with the initial version of KFX and some thoughts on where to improve.

6.4.1 Near surface dispersion

While dispersion of a neutrally or positively buoyant gas will be strongly dependent on how the entire flow field is behaving, denser-than-air gases will stay close to the ground for a relatively long time, and is thus much more dependent on the turbulence characteristics close to the ground. In this respect, one discomforting feature of the results presented in this chapter is their high error-values in the regions close to the ground (see, for instance, Fig. 6.6). A too small turbulence related viscosity will diffuse the gas slower than it should, and the concentrations will stay higher and closer to the ground.

While the Monin-Obukhov theory is not meant for the "roughness" layer, these simulations were done with a uniform, smooth surface. The boundary values themselves might therefore be wrong in this region, but it is nevertheless wanted with a *decreasing* eddy viscosity in the lower wind field.

With the results from the Thorney Island trials, a too small turbulence related viscosity does not seem to be the problem, rather the opposite. In this thesis, however, the object is to look at dense gas dispersion in the atmosphere as a whole, and then a wind field correctly maintained over a large distance is important.

One explanation for the exaggerated spreading of the gas over the fence could be the use of a too low turbulence Schmidt number. This is examined in the next chapter.

6.4.2 Laterally homogeneous

It is not unexpected that the boundary layer seems to have a development through the calculation domain. If the ground is modeled as a flat plate, and the surrounding flow enters the plate undeveloped, it is expected for a turbulent boundary layer to grow. Ertesvåg (2000, p. 78) notes that the standard values for the model constants, Table 4.1 are shown to give adequate results for, among other scenarios, the *development* of a boundary layer along a flat plate.

When modeling the atmospheric boundary layer, it must be seen from a different view. As lateral directions tends to infinity, as is the case for boundary layer flows along a comparatively large sphere, there should be no gradients along the flow lines. Or "the averaged characteristics of the flow in this system are a function only of the vertical coordinate z" (Monin & Obukhov, 1954). This is clearly not the case for a boundary layer developing over a finite flat plate, as is the scenario the k-ε model is adjusted for.

6.4.3 Boundary layer height

Equation (3.16) approximates the boundary layer heights in a neutral or stable atmosphere, which corresponds well with the atmospheric boundary layer height of $3 \cdot 10^3$ m given by Tennekes & Lumley (1972, p. 12). The calculation domains used in these simulations are of height 150 m and (to provide a control of the results) 500 m, which means that the domain heights might very well surpass the surface layer depths of similar actual scenarios.

CFD modeling is used on problems of increasing size, large scale gas dispersion being the most prominent example. Using other boundary conditions than the surface layer similarity theories do not seem to have been given focus in the research thus far, so the implications of having domains which are taller than 10% of h are unknown. It is, nevertheless, a reminder to take the "correctness" of the Monin-Obukhov profile with a grain of salt, both at its near surface values, and the values highest in the domain, since these would normally be outside the surface layer.

6.4.4 Non-locality

Figure 6.7 presents the three-dimensional energy spectrum and the dissipation rate spectrum. Here, κ is an inverse length scale, the wave number. Averaged over a relatively short time period, these spectra show how the mean turbulence kinetic energy and its dissipation rate are distributed over different length scales, where most of the kinetic energy is in the larger length scales (i.e. small κ) and most of the dissipation occurs in the smaller, molecular viscosity-affected length scales, as is expected.

k and ε can then be found by integrating across all wavenumbers. For k, in an isotropic scenario, this is expressed (Ertesvåg, 2000)

$$\int_0^\infty E(\kappa, t)\, d\kappa = k(t), \tag{6.1}$$

where both the distributions of k and ε are shown in Fig. 6.7.

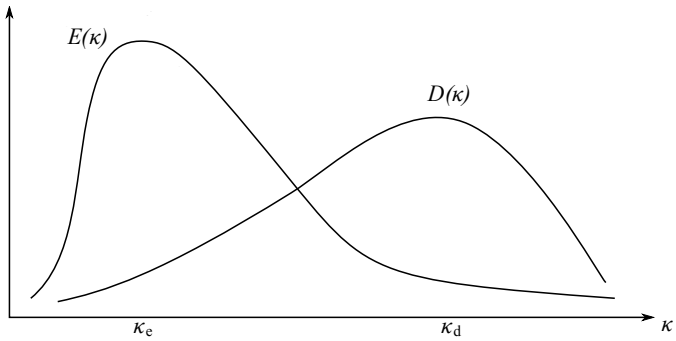

Figure 6.7: The energy and dissipation rate spectra, adapted from Ertesvåg (2000, Fig. 8.5)

For boundary layer flows, the largest length scales are confined by the surface and the boundary layer height. This means that for an atmospheric boundary layer, the largest length scales are in the same order of magnitude as h. The smallest turbulence length scales are defined by the Kolmogorov length, η. The ratio between the largest and smallest length scales is a function of the Reynolds number, and is expressed (Tennekes & Lumley, 1972, p. 21)

$$\frac{\eta}{l} \sim \mathrm{Re}^{-3/4}. \tag{6.2}$$

From this alone, it can be argued that the k-ε model is better suited for a high-Reynolds number scenario, where there is a clear separation between κ_e and κ_d (from Fig. 6.7).

Gas dispersion in the atmosphere is a flow situation where there may be substantial amounts of turbulence energy in both longer and shorter scales. The atmospheric flow itself has most of its turbulence energy in large eddies, whereas a turbulent gas flow contains physically much smaller currents. In this situation, the $E(\kappa)$ and $D(\kappa)$ curves can appear smeared out, a distribution that is difficult for the k-ε model to accurately describe. One approach to solve this might be to have two "levels" of turbulence models, where the dissipation term in the upper level, is the production term in the lower. This would result in two scalar length scales, and the possibility to have a better representation of the dimensions.

Richards & Norris (2011) note on the use of the k-ε model on atmospheric boundary layers, that the source of error between calculations and the observed profiles is "primarily contributed by very large eddies that are not reflected in the modelled turbulence," which supports the point made here. As long as a separate model for the atmospheric flow is not used, this will be a problem for the software. As stated earlier, the alterations in KFX must prevail the generality of the models, and it has been tried to find different means of handling the model's problems with atmospheric flows.

6.4.5 Modeling the surface with porosity layers

The surface for the Thorney Island releases had "an aerodynamic roughness of 10-20 mm corresponding to rough grassland" (McQuaid & Roebuck, 1985). While the effect of the grass is included through the roughness scaling height, z_0, and the surface roughness in the calculation domain, the ability of the grass to withhold the gas is not included in the modeling.

This might explain some of the aspects of the simulation results. That the gas in the actual trials seems to linger on the upwind side of the fence, could be because a substantial amount of it is dispersed into the grass layer and then gradually seeping out. To get this effect in a mathematical modeling, one alternative would be to have a layer of porous cells next to the ground. Porous cells are cells with a solid fraction less than one, and one of their effects is to work as resistances to flow. This alternative is not examined further here, but is one suggestion for further work.

7 Alterations to the modeling

The version of the k-ε model that is used in KFX is already thoroughly validated in its typical area of use. As previously mentioned, KFX is meant to be applicable to a number of different scenarios, and for most of them the wind field is not even a major contributor to the uncertainty. This means that any alterations made to the turbulence modeling in KFX has to be slight and unobtrusive, so that the results in other parts of the simulation are as unaffected as possible.

In this chapter, three alterations are suggested and they are compared with either the Thorney Island scenario, the empty wind field or both.

7.1 Considerations and proposed alterations

Some considerations have to be made before any alterations can be applied on models. There are suggested three alterations to the existing models, each meant to cover a separate problem area.

7.1.1 Unobtrusiveness

A main criteria for the alterations has to be that they are as unobtrusive as possible. Any existing, well-validated results by KFX has to remain effectively unaltered after the modifications to the dense gas handling are applied. This therefore excludes static modifications to the model constants, or any similar approach, as this would devaluate other simulations done in KFX.

Unobtrusiveness adds to the challenge of finding a good improvement to the model, and emphasize the point that as more is demanded of one software package it gets harder to model each part accurately, which is is also a point in the argument to initially use a simpler, dedicated code for the alterations first. This was not done in the work on this thesis, where alterations were implemented in KFX directly.

7.1.2 The range of scales

As stated in Ch. 2, a dense gas release develops through several phases, all of which lay different demands on the models. The outer points on this continuum are, on the one hand, the initial phase, where the gas' negative buoyancy has a clear influence on the dispersion; and, on the other, the far-field effect of the dispersion being controlled by the wind and its turbulence characteristics.

Three alterations are tested here, each meant to cover a different area on this range. First a modification to the turbulence Schmidt number, $\sigma_{\widetilde{Y}_l t}$, is tested, with

the hope to improve on the tendency of the gas to surpass obstacles too quickly. Next, a function variation to one model constant, C_1, is implemented to account for "large scale effects" (Baklanov, 2000) of the atmospheric dispersion. The aim here is to first improve upon the modeling of the atmospheric flow, then see how this affects near-release dense gas behavior. Finally, an additional term is introduced to the transport equations for k and ε. These productions terms are included to force consistency with Monin-Obukhov theory while still allow for other, more high-intensity turbulence effects to remain unaffected.

Among the three, only the final approach gives results that warrant further examination.

7.2 Turbulence Schmidt number

Andronopoulos *et al.* (1994) argue that in a stably stratified flow, as that in a dense gas cloud, movement of the gas by turbulence is inhibited, whereas the turbulent motions may still travel by internal waves. Their suggested approach is meant for the *k-l* model used in Adrea-HF, but the theory behind it should be just as applicable in KFX. Note that the inclusion of a varying $\sigma_{\widetilde{Y}_l t}$ comes together with a buoyancy driven production in their model as well. This means that the G terms in Eqs. (4.43) and (4.44) are kept unchanged.

7.2.1 Implementation

The Richardson number is calculated according to Eq. (4.12), here using central differencing schemes for both the velocity and the density gradients. To ensure that the procedure would not interrupt any other flow parameter, a criteria of a gas concentration higher than 2% was used before the value was calculated. A simple iteration process was used to find $\sigma_{\widetilde{Y}_l t}$, Eq. (4.10), with a convergence criteria of $(\sigma^{n+1}_{\widetilde{Y}_l t} - \sigma^{n}_{\widetilde{Y}_l t})/\sigma^{n}_{\widetilde{Y}_l t} < 0.05$, where n is the iteration step number.

The calculations were done using flow values of the prior time step, even if the transport equation for $\widetilde{Y}_l$ is not solved until the final step (see Fig. 5.1). This guarantees the gas is not moved by gradients that occurred during the current time step.

7.2.2 Results

Figure 7.1 shows the development of the concentration profiles in two closely positioned measuring points (Fig. 6.1), MP 1 and MP 2. Collectively these results show a trend for the gas to be concentrated in a narrower cloud. As the Schmidt number increases, the gas is transported less by turbulence, which in addition to transporting it upwards also transports it to the sides. Therefore the gas follows the bulk motion of the air, which leads to the center of the fence. This negative impact of this approach, that the model now dampens the diffusive transport in all directions, was not obvious prior to seeing the data.

As is shown in Fig. 7.1, the concentrations are higher all over, since the increased turbulence Schmidt number prohibits dilution. However, it also inhibits diffusion

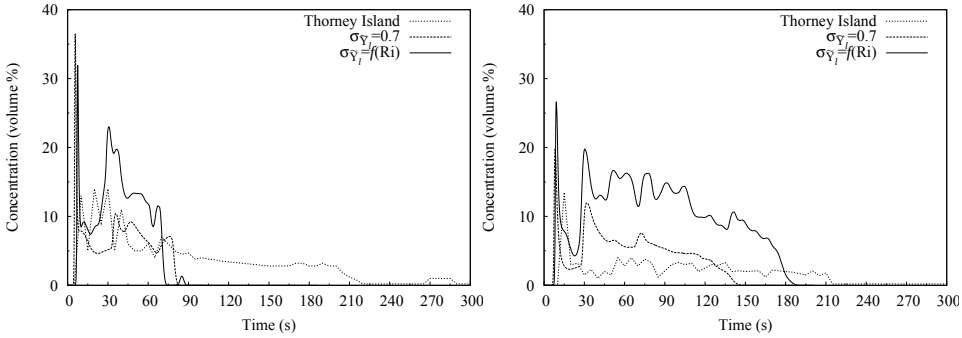

(a) Measuring point 1 (b) Measuring point 2

Figure 7.1: Development of gas concentration using $\sigma_{\widetilde{Y}_l t}(\mathrm{Ri}_f)$

in the lateral directions and this effect is shown in Fig. 7.1a, where the gas now leaves the area, following the bulk wind movement, quicker than it did when the diffusion helped its transport in this cross-wind direction.

7.2.3 The buoyancy related production

The turbulence Schmidt number influence the flow in a surprising manner. The increase in $\sigma_{\widetilde{Y}_l t}$ was suspected to make the gas stay on the upwind side of the fence for a longer period, an effect that occurred at just one measuring point. This could be due to how the eddy viscosity behaves in the dense gas plume, an area where the buoyancy driven production, G, works to dampen the turbulence level.

To get a qualitative view of these terms' effect, one simulation was done with them disabled, while having all other terms at their standard values. As C_3 is zero either way in a dense gas cloud, the effect is merely deactivating a term in the transport equation for k. The results of deactivating this term is shown in Fig. 7.2. Between the two, Fig. 7.2a proves that G works to suppress μ_t by at least an order of magnitude compared to Fig. 7.2b in the area with dense gas.

The use of an explicit buoyancy driven production in an otherwise Favre averaged transport equation, as it appears in KFX, is undocumented. When using Favre averaged quantities, the external force f_i disappears since $\overline{\rho u_i''} f_i = 0$ (Ertesvåg, 2000, p. 231). This is not to say that the gravity no longer influence the solution, but it contributes through other terms in the equations (e.g. pressure and momentum). One could argue that the application in KFX is a modeling of the pressure or momentum effect through the external force. This means moving one step towards the standard equations using Reynolds averaged quantities. This is not necessarily unwanted, as long as the right physical effects still are accounted for in the equations.

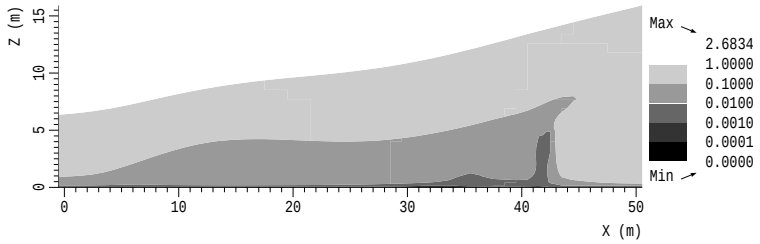

(a) With G

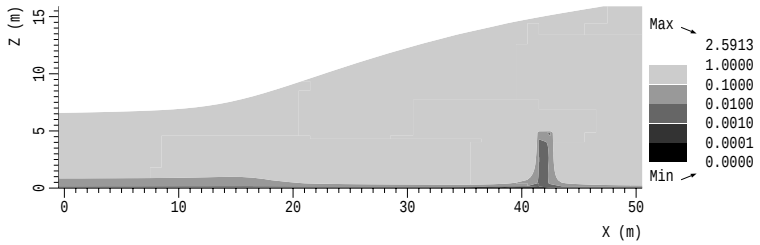

(b) Without G

Figure 7.2: Iso-contours for $\mu_t$with and without G at xz-plane with measuring point 1, 40 seconds after release

7.2.4 Anisotropy

Pereira & Chen (1996) mention a similar, perhaps more sophisticated approach than the modified $\sigma_{\widetilde{Y}_i t}$, using anisotropic turbulence related viscosity and diffusivity. Used together with a modified model constant, C_3, this is meant to account for "the strong anisotropy of turbulent diffusion encountered in stratified flows close to the ground." The aim is then to include similar phenomena as those with a modified turbulence Prandtl-Schmidt number. In addition, using an anisotropic viscosity and diffusivity could help create a wider plume that would still be inhibited from vertical diffusion.

This procedure is not tested here, but it is suggested as future work. A turbulence Schmidt number modification as that tested here is a small intrusion in KFX, and can be implemented without much restructuring of the current code. Implementing an anisotropic eddy viscosity would, however, require substantial reconfiguration of today's setup, and is thus probably best tested with a simpler, dedicated code.

7.3 Flow dependent model constant

One of the suggested areas of future work from the specialization project was to try Baklanov's (2000) proposed improvement of the model constant C_1. While used with a slightly different similarity theory for the wind field, this was meant to improve the k-ε model's handling of non-local turbulence effects.

Please note that the procedure tested here is not intended to be an assessment of the function itself, merely of the use of it in KFX.

7.3.1 Implementation

The revised constant is a function of turbulence and atmospheric quantities, in addition to an empirically based constant d_h, adjusted here by finding a point where it leads to a reasonably small degradation of μ_t. The new function is then expressed

$$C_1' = C_1 \frac{C_\mu k^{3/2} f^{1/2}}{\varepsilon d_h (u_* L)^{1/2}}. \tag{7.1}$$

This is implemented in KFX by calculating the new value for each time step based on the local values in the prior. Knowing that the standard value is $C_1 = 1.44$, it is assumed that C_1' should, on average, be close to this.

Keeping C_1 and C_μ at their standard values, Eq. (7.1) leaves only d_h to be set through a parameter study. The Coriolis parameter, f, is calculated in accordance with Sec. 3.3.2 (p. 18).

7.3.2 The empty wind field

The purpose of this function is first and foremost to improve KFX's dense gas treatment *indirectly* through an improved wind field. Since the available experimental data for comparison here corresponds to a neutral atmospheric stability, this is also the configuration used in the tuning of d_h.

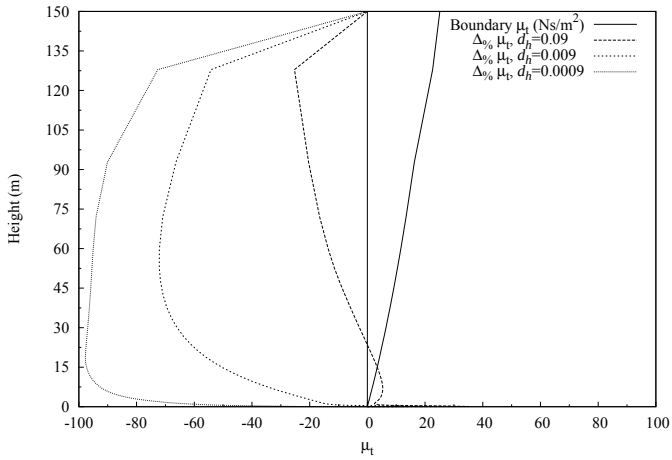

Figure 7.3: Parameter study for d_h, 900 m downstream

Figure 7.3 shows the dependency of d_h 900 m downwind. Starting with Baklanov's (2000) suggested value of $d_h = 0.0009$, gives a complete destruction of the

eddy viscosity. This is due to C_1 in Eq. (4.44) now being much too large, resulting in an unrealistic production of ε. Reducing C_1' by incrementally increasing to $d_h = 0.09$ gives a satisfying outcome, where the average C_1' was at a comforting 1.56 across all cells. The deviation from the boundary value of μ_t is still relatively large, but the tendency to get a positive error in the lower parts is taken as a signal to not increase the value further.

7.3.3 Influence on dense gas dispersion

Baklanov's (2000) function is aimed at improving the gas dispersion characteristics of the k-ε model's treatment of large scale atmospheric boundary layers. Therefore, the hope is that it will not affect the near-release dispersion of dense gas seen in the simulated Thorney Island trial.

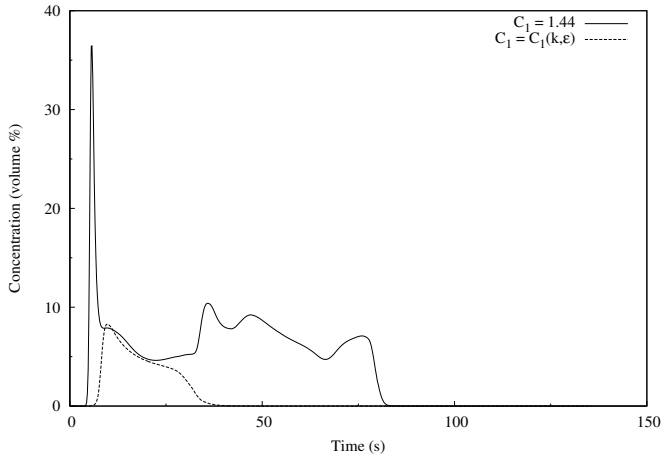

Figure 7.4: Thorney Island trial 21 with C_1', measuring point 1

Figure 7.4 shows how the new C_1' leads to a far faster dispersion of the gas at measuring point 1. The physical explanation for this could be that C_1', which now averages to a value of 0.91, is too small, leading to a smaller production of ε thus a higher eddy viscosity and faster dispersion of the gas.

Of the three suggested alterations here, this is the least promising. As mentioned, this attempted use differs from Baklanov's (2000) suggested implementation, a problem that tuning d_h was meant to treat. The results presented in Fig. 7.4 give no incentive for further tests of this in KFX.

7.4 Correctional production

The third and final alteration to the current model is a production term meant to maintain the atmospheric boundary layer.

7.4.1 Justification

Richards & Norris (2011) comment on how the values of k obtained with the k-ε model differ from those typically observed in the atmosphere. Such observations also show a tendency for k to vary with height, present as a z-dependency in Eq. (3.14).

As tested previously in this chapter, one approach could be to alter the model constants in such a way that the transport equations become consistent with the theory's boundary values. This entails collecting a database of new values for, for instance, σ_k and σ_ε, values that would only be valid for specific configurations.

This will always be a challenge with a code as diverse in use as KFX, to balance generality of the models and still give satisfying results in each scenario. The solution suggested here is to have a weak correctional production. This is meant to "push" an unobstructed wind field to its laterally homogeneous solution. Note that these results will never be better than the boundary values that are used (i.e. the applied atmospheric similarity theory).

7.4.2 Expression

Using $\Delta\phi$ to denote the difference between the known boundary and the local value of a flow scalar ϕ ($\Delta\phi = \phi_{\text{m-o}} - \phi$), the production terms can be introduced into Eqs. (4.43) and (4.44) as

$$\frac{\partial \bar{\rho} k}{\partial t} + \frac{\partial (\bar{\rho} \tilde{u}_i k)}{\partial x_i} = \frac{\partial}{\partial x_i} \left(\left(\mu + \frac{\mu_t}{\sigma_k} \right) \frac{\partial k}{\partial x_i} \right) + \bar{\rho} P - \bar{\rho} \varepsilon + G + \bar{\rho} M_k \tag{7.2}$$

and

$$\begin{aligned} \frac{\partial \bar{\rho} \varepsilon}{\partial t} + \frac{\partial (\bar{\rho} \tilde{u}_i \varepsilon)}{\partial x_i} =& \frac{\partial}{\partial x_i} \left(\left(\mu + \frac{\mu_t}{\sigma_\varepsilon} \right) \frac{\partial \varepsilon}{\partial x_i} \right) + \\ & C_1 f_1 \bar{\rho} P \frac{\varepsilon}{k} - C_2 f_2 \bar{\rho} \frac{\varepsilon^2}{k} + C_1 C_3 \frac{\varepsilon}{k} G + \bar{\rho} M_\varepsilon, \end{aligned} \tag{7.3}$$

using M_k and M_ε as the new production terms, expressed

$$M_k = f(\Delta k) \frac{1}{\tau_M} \tag{7.4}$$

and

$$M_\varepsilon = g(\Delta \varepsilon) \frac{1}{\tau_M}, \tag{7.5}$$

where f and g are arbitrary functions of the same dimension as k and ε respectively. τ_M is a model time scale to ensure dimensional consistency.

After integrating over a cell's volume, per the standard FVM procedure, τ_M relates to a volume flow of k or ε, meaning that M_ϕ expresses a source or a sink of ϕ, depending on its sign. Finding an expression for this time scale must be solved first.

7.4.3 Time scale

Integrating over the cell volume and including the density, results in a numerical time scale

$$a_\tau \sim \frac{\bar{\rho}\Delta V}{\tau_M}. \tag{7.6}$$

As there is no obvious physical explanation for τ_M, there is not one for a_τ either. Two approaches to the problem of expressing a_τ are tested here. The first is using a_τ as the "sum of the neighbor coefficients," $a_\tau = \sum a_{\text{nb}}$. The second is to express a_τ through a mass flow related to the wind,

$$a_\tau = \frac{1}{2}\sum \rho_a |\bar{u}_{10i}| \mathrm{A}_{\mathrm{x_i}}, \tag{7.7}$$

using that $|\bar{u}_{10i}|$ is the wind's velocity at a reference height 10 m above the surface in the x_i-direction and $\mathrm{A}_{\mathrm{x_i}}$ is the cell's surface area normal to the same direction.

One strength of Eq. (7.7) is that a_τ will behave predictably across all cells, with the weakness of not reflecting the local gradients. As will be seen, both variations lead to satisfying results.

7.4.4 Form of the functions

The performance of this model is bound to depend on the chosen functions f and g. These have to be linearized before they are used, see Eq. (5.13). Since $k_{\text{m-o}}$ and $\varepsilon_{\text{m-o}}$ are static functions, it is easiest to use linear proportional expressions for f and g,

$$f(\Delta k) = C_k(k_{\text{m-o}} - k) \qquad \text{and} \qquad g(\Delta\varepsilon) = C_\varepsilon(\varepsilon_{\text{m-o}} - \varepsilon), \tag{7.8}$$

which enters the source terms as

$$S_{C,k} = C_k k_{\text{m-o}} a_\tau \qquad \text{and} \qquad S_{P,k} = C_k a_\tau \tag{7.9}$$

for M_k and

$$S_{C,\varepsilon} = C_\varepsilon \varepsilon_{\text{m-o}} a_\tau \qquad \text{and} \qquad S_{P,\varepsilon} = C_\varepsilon a_\tau \tag{7.10}$$

for M_ε, where C_k and C_ε are model constants.

M_k and M_ε then need to be small enough to be neglected when there are other, more influential sources of turbulence, or other reasons for large Δk and $\Delta\varepsilon$, as that in a dense gas cloud.

The coming results show that this was not an issue in the Thorney Island simulation, and the matter is not looked further into here. A suggested future work is to see have the proposed functions affects combustion simulation, or other high turbulence intensity flows. M_k and M_ε could then be "deactivated" in these regions by inclusion of a factor that tends to zero as the deviations increase.

The influence of M_k and M_ε is meant to be slight, and gradually working over longer distances, maintaining as low Δk and $\Delta\varepsilon$ as feasible.

7.4.5 Empty wind field

As this alteration is meant to improve the k-ε model's handling of the wind field, it is first and foremost assessed and validated through simulations done in the empty wind field scenario.

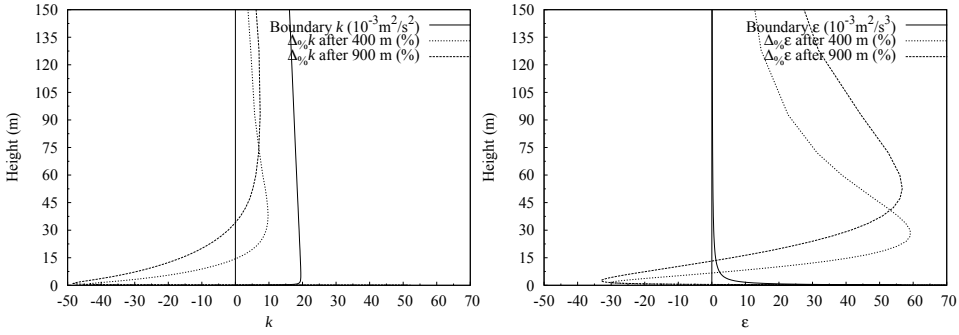

(a) k (b) ε

Figure 7.5: Percent wise change in k and ε, without M

Without any alterations to the models, the k and ε profiles develop as depicted in Fig. 7.5. The error in k appears to be less significant than that in ε, and the latter is what sets the overall declining trend for μ_t, as seen in Fig. 6.6a (p. 50).For simplicity, the model constants in Eqs. (7.9) and (7.10) are kept equal. They do, nevertheless, depend on the chosen configuration of a_τ.

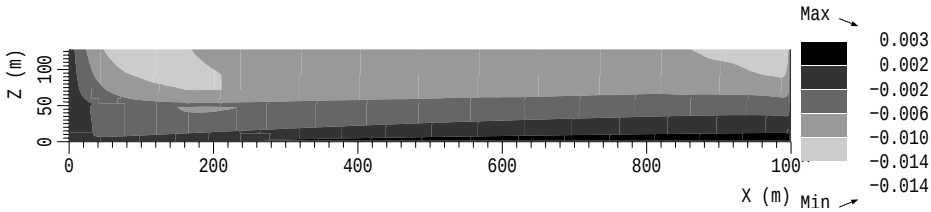

(a) $C_k = 0.005$, $C_\varepsilon = 0.005$, $a_\tau = \sum a_{\mathrm{nb}}$

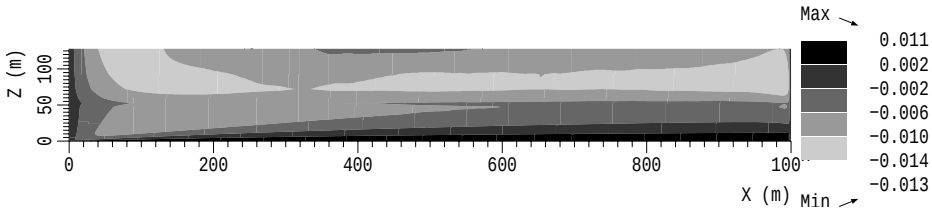

(b) $C_k = 0.100$, $C_\varepsilon = 0.100$, $a_\tau = |\bar{u}_{10i}|\mathrm{A}_{\mathrm{x_i}}\rho_a$

Figure 7.6: M_k

Figure 7.6 presents the iso-contours for M_k with the two different variations of a_τ. The profiles are similar, the two discernible difference are more gentle transitions in Fig. 7.6a and that there is a x-gradient in M_k in Fig. 7.6b. The values of C_k and C_ε in the two scenarios are adjusted in such a way that the product of the average a_τ and the constants are similar between the cases.

As both configurations of a_τ give a destruction of k in the higher parts of the domain and vice versa, M_k occurs to behave as expected.

The resulting developments are shown in Fig. 7.7, where the differences between the two are more apparent. Both deviation curves are now down to negligible values for higher z-values, while $a_\tau = \sum a_{\mathrm{nb}}$ results in a better behavior close to the surface, this is therefore kept as the standard configuration.

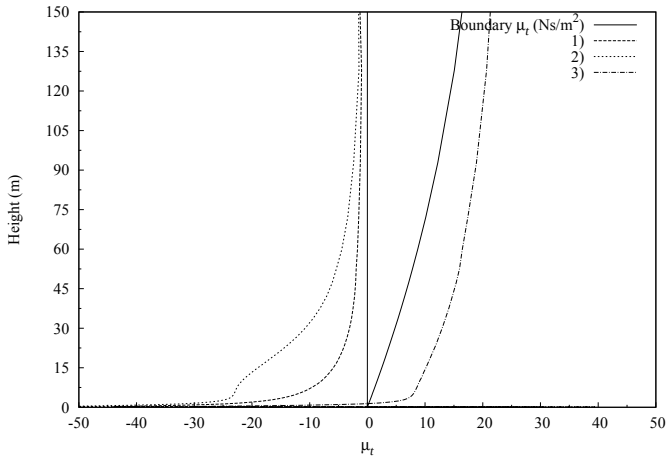

Figure 7.7: The effect of different a_τs, 1) and 2) correspond to Figs. 7.6a and 7.6b, respectively. 3) is for super-critical model constants.

Note that there is still a non-zero deviation in the upper parts, due to the chosen function form of f and g. Balchen *et al.* (2003) state that such use of what is, in effect, a proportional controller will always leave an error, since the error must be there for the controller to be active. It is also clearly dependent on the values of the model constants, and setting C_k and C_ε above some critical values can lead to oscillations. This is shown in the line marked 3) in Fig. 7.7, where the percentage wise deviation is *positive* towards the end of the domain. That calculation was done with $C_k = C_\varepsilon = 0.05$, ten times those used to get line 2) in Fig. 7.7.

7.4.6 Thorney Island

Since this modification is aimed at improving the wind modeling far downstream, it is not expected to better the direct near-source dispersion of dense gas. The hope is, however, that the correction productions' contributions are so small that they have no substantial effect on these near-field dispersion results.

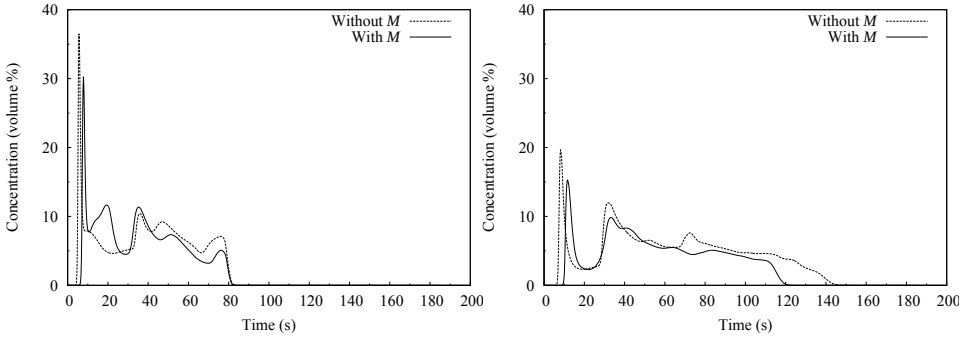

(a) Measuring point 1 (b) Measuring point 2

Figure 7.8: Influence of M_k and M_ε on the Thorney Island simulation

The chosen linearly proportional f and g are nevertheless expected to have a noticeable impact in areas where the absolute deviations are high. The chosen points of interest, measuring point 1 and 2, are in areas where there is an initial high turbulence intensity due to the fence, an intensity that more or less disappears as the gas enters this region (see Fig. 7.2a, p. 58). This means that at no point during the simulation are M_k and M_ε meant to be be active in these areas.

Considering this, the results in Fig. 7.8 indicate that shear and buoyancy related production will dominate in these regions. The development of the gas profiles therefore show similar trends both with and without the correctional productions active.

One conclusion in this section is that using such a production term seems beneficial in dense gas releases. While it gives a significant improvement of the wind field modeling, it does not interfere with the near release dense gas dispersion itself.

This concludes what will be the recommended implementation of M in KFX. The following section test a hypothesis regarding the treatment of the lower boundary conditions.

7.4.7 Imbalance near surface

The k-ε model's difficulties to adequately describe atmospheric boundary layers have already been validated. Richards & Norris (2011) and Sumner & Masson (2009) all elaborate on the possibility that one main source of error could be an inconsistency in how P and ε are treated in the near-wall cells. This means that the problem is not entirely caused by the k-ε model itself, but how it is numerically implemented in a FVM-based CFD software.

While Sumner & Masson (2009) improve the model by including a grid-specific correction factor to the production and dissipation rate terms, the theory is tested in KFX in a different manner. The assumption is that forced consistency only in the lower-most cells, through use of M_k and M_ε, should contribute substantially to the rest of the domain.

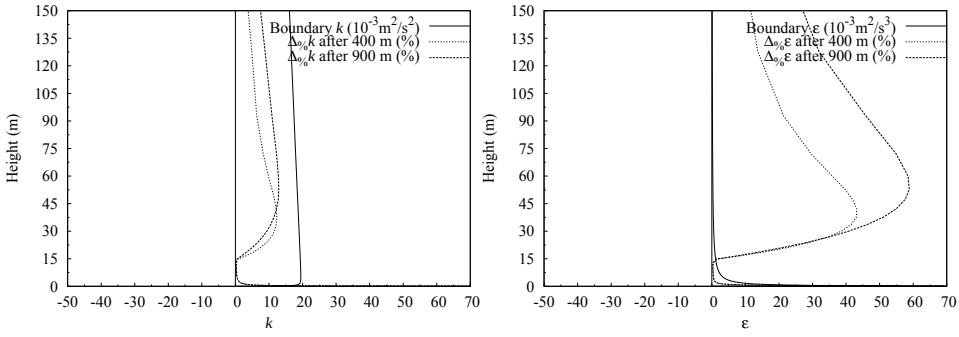

(a) k profile (b) ε profile

Figure 7.9: $M_\phi(z > 15m) = 0$, with C_k and $C\varepsilon$ of values 0.005

Figure 7.9 shows that this is not realized. Here M_k and M_ε removes the error in the lowest 15 m, but the deviations soar upwards as soon as the correctional productions are deactivated. Therefore, the problem present here does not lie in the griding or lower boundary conditions, but in an inconsistency in the k-ε model itself.

The suggested procedure is then to keep the production terms active in the entire domain.

7.4.8 Comments

In this section, a correctional production term proved to be beneficial for atmospheric boundary layer problems. The new terms acted unobtrusive towards the already established flow scenarios, while increasing the accuracy of the far field modeling.

8 Conclusion

Using the k-ε model on a wider and wider scope of scenarios, means that the standard set of constants has to account for an increasing number of physical effects.

8.1 Concluding remarks

Gas dispersion problems in the atmosphere are typical examples of cases where the energy spectra will tend to a non-ideal setup for the k-ε model, especially if one still expects it to perform well under its typical use.

Three alterations have been tested on the current set of mathematical models used in KFX. One was dedicated to the near-release spreading of the dense gas, one a modifications to the model constants and finally an introduction of new correctional production terms in the transport equations for both k and ε. Of the three, the third was the only to give results good enough to warrant further investigation.

This approach improved noticeably upon the k-ε models handling of the wind field. The untreated model equations result in a decreasing eddy viscosity through the calculation domain when modeling a neutral atmospheric boundary layer. The correctional productions removes most of this error, depending on the chosen model constants.

It was shown that the decreasing profiles was not due to unwanted treatment of the lower boundary values, but an inconsistency in the turbulence modeling itself, as expected.

8.2 Future work

The work done for this thesis could be used as part of a foundation for future work, where some of the following is suggested to be examined further:

- Both this thesis and the specialization project use an un-reacting, iso-thermal gas. Several dense gas effects are not considered, which would be present if a more complex scenario was modeled. An interesting area of study, could be a combination of LNG pool spreading, with a focus on the resulting large scale dense gas release.
- Try an anisotropic version of the eddy viscosity to improve the treatment of the dense gas flow. This is probably best done through a simpler, dedicated model.

- Use profiles for the atmospheric boundary layer that are also valid for unstable stratification. Both this and the treatment of dense gas flow could call for a review of the buoyancy generation used in KFX. The use of a height-varying temperature field could also be looked into.
- Try different variations for the parameters used in the correction production terms M_k and M_ε. These are, as of now, far from optimized.

References

Andronopoulos, S., Bartzis, J., Würtz, J. & Asimakopoulos, D. 1994 Modelling the effects of obstacles on the dispersion of denser-than-air gases. *Journal of Hazardous Materials* **37**, 327 – 352.

Arya, S. P. 2005 Micrometeorology and atmospheric boundary layer. *Pure and Applied Geophysics* **162**, 1721–1745.

Bærland, T. 2010 Dense gas dispersion: A comparison between KFX and Thorney Island phase II data. *Tech. Rep.*. NTNU.

Baklanov, A. 2000 Application of CFD methods for modelling in air pollution problems: Possibilities and gaps. *Environmental Monitoring and Assessment* **65**, 181–189.

Balchen, J., Andresen, T. & Foss, B. 2003 *Reguleringsteknikk*, 5th edn. Institutt for teknisk kybernetikk.

BP 2010 BP Statistical Review of World Energy June 2010. http://www.bp.com/sectiongenericarticle.do?categoryId=9023753&contentId=-7044109. Accessed: 06/06/2011.

Brambilla, S., Manca, D., Williams, M., Gowardhan, A. & Brown, M. 2009 *A shallow water model for dense gas simulation in urban areas*. Los Alamos National Laboratory.

Briggs, G. A., Britter, R. E., Hanna, S. R., Havens, J. A., Robins, A. G. & Snyder, W. H. 2001 Dense gas vertical diffusion over rough surfaces: results of wind-tunnel studies. *Atmospheric Environment* **35**, 2265 – 2284.

Britter, R. & Griffiths, R. 1982 The role of dense gases in the assessment of industrial hazards. *Journal of Hazardous Materials* **6**, 3 – 12. Dense Gas Dispersion.

Britter, R. & McQuaid, J. 1988 Workbook on the dispersion of dense gases. *HSE contract research report Sheffield* .

Britter, R. E. 1989 Atmospheric dispersion of dense gases. *Annual Review of Fluid Mechanics* **21**, 317–344.

Daish, N., Britter, R., Linden, P., Jagger, S. & Carissimo, B. 2003 Smedis: scientific model evaluation of dense gas dispersion models .

Danielsen, H. 2000 ComputIT – ny knoppskyting fra NTNU/SINTEF Energiforskning. http://www.energy.sintef.no/publ/xergi/2000/2/art-13.htm. Accessed: 14/12/2010.

Duynkerke, P. G. 1988 Application of the e – ε turbulence closure model to the neutral and stable atmospheric boundary layer. *Journal of the Atmospheric Sciences* **45** (5), 865–880.

Ellison, T. H. & Turner, J. S. 1960 Mixing of dense fluid in a turbulent pipe flow part 2. dependence of transfer coefficients on local stability. *Journal of Fluid Mechanics* **8** (04), 529–544.

Ertesvåg, I. 2000 *Turbulent strøming og forbrenning*, 1st edn. Tapir akademiske forlag.

Freedman, F. R. & Jacobson, M. Z. 2003 Modification of the standard ε-equation for the stable ABL through enforced consistency with Monin-Obukhov similarity theory. *Boundary-Layer Meteorology* **106**, 383–410. 10.1023/A:1021251523246.

Funada, T. & Joseph, D. 2001 Viscous potential flow analysis of Kelvin-Helmholtz instability in a channel. *Journal of Fluid Mechanics* **445**, 263–283.

Han, J., S.P., A., Shen, S. & Lin, Y.-L. 2000 An estimation of turbulent kinetic energy and energy dissipation rate based on atmospheric boundary layer similarity theory. *Tech. Rep.* CR-2000-210298. NASA.

Hinze, J. 1975 *Turbulence*, 2nd edn. McGraw-Hill Publishing Company.

Huser, A., Nilsen, P. J. & Skåtun, H. 1997 Application of k-ε model to the stable ABL: Pollution in complex terrain. *Journal of Wind Engineering and Industrial Aerodynamics* **67-68**, 425 – 436. Computational Wind Engineering.

Jones, W. & Launder, B. 1972 The prediction of laminarization with a two-equation model of turbulence. *International Journal of Heat and Mass Transfer* **15** (2), 301 – 314.

Launder, B. E. & Spalding, D. B. 1974 The numerical computation of turbulent flows. *Computer Methods in Applied Mechanics and Engineering* **3** (2), 269 – 289.

Lilleheie, N. 2011 *Extended shallow-layer pool model in KFX 2010 LNG*. ComputIT AS.

Luketa-Hanlin, A., Koopman, R. P. & Ermak, D. L. 2007 On the application of computational fluid dynamics codes for liquefied natural gas dispersion. *Journal of Hazardous Materials* **140** (3), 504 – 517. LNG Special Issue - Dedicated to Risk Assessment and Consequence Analysis for Liquefied Natural Gas Spills.

Maele, K. V. & Merci, B. 2006 Application of two buoyancy-modified k-[epsilon] turbulence models to different types of buoyant plumes. *Fire Safety Journal* **41** (2), 122 – 138.

Mahrt, L. 1999 Stratified atmospheric boundary layers. *Boundary-Layer Meteorology* **90**, 375–396.

McNaughton, K. 2009 The rise and fall of Monin-Obukhov theory. *AsiaFlux Newsletter* **30**.

McQuaid, J. 1985 Objectives and design of the phase I heavy gas dispersion trials. *Journal of Hazardous Materials* **11**, 1 – 33.

McQuaid, J. & Roebuck, B. 1985 Large scale field trials on dense vapour dispersion. *Commision of the European communities* .

Melhem, G., Saraf, S. & Ozog, H. 2006 LNG Properties and Hazards: Understand LNG Rapid Phase Transition (RPT). *Tech. Rep.*. ioMosaic Corporation.

Monin, A. & Obukhov, A. 1954 Basic laws of turbulent mixing in the surface layer of the atmosphere. *Trudy Geofiz. Inst. AN SSR* **24** (151), 163–187.

Obukhov, A. M. 1971 Turbulence in an atmosphere with a non-uniform temperature. *Boundary-Layer Meteorology* **2**, 7–29. 10.1007/BF00718085.

Ohba, R., Kouchi, A., Hara, T., Vieillard, V. & Nedelka, D. 2004 Validation of heavy and light gas dispersion models for the safety analysis of LNG tank. *Journal of Loss Prevention in the Process Industries* **17** (5), 325 – 337.

Pahlow, M., Parlange, M. B. & Porte-Agel, F. 2001 On Monin-Obukhov similarity in the stable atmospheric boudary layer. *Boundary Layer Meteorology* **99** (2), 225–248. 99: 225-248.

Patankar, S. 1980 *Numerical Heat Transfer and Fluid Flow*. McGraw-Hill Book Company.

Patel, V. C., Rodi, W. & Scheuerer, G. 1985 Turbulence models for near-wall and low Reynolds number flows - A review. *AIAA Journal* **23**, 1308–1319.

Pereira, J. C. F. & Chen, X. Q. 1996 Numerical calculations of unsteady heavy gas dispersion. *Journal of Hazardous Materials* **46** (2-3), 253 – 272. Heat and Mass Transfer in Chemical Process Industry Accidents.

Peters, W. D., Cogswell, S. R. & Venart, J. E. S. 1996 Dense gas simulation flows over rough surfaces. *Journal of Hazardous Materials* **46**, 215 – 223. Heat and Mass Transfer in Chemical Process Industry Accidents.

Richards, P. & Norris, S. 2011 Appropriate boundary conditions for computational wind engineering models revisited. *Journal of Wind Engineering and Industrial Aerodynamics* **99** (4), 257 – 266. The Fifth International Symposium on Computational Wind Engineering.

Rottman, J. W., Hunt, J. & Mercer, A. 1985*a* The initial and gravity-spreading phases of heavy gas dispersion: Comparison of models with phase I data. *Journal of Hazardous Materials* **11**, 261 – 279.

Rottman, J. W., Simpson, J. E., Hunt, J. & Britter, R. 1985*b* Unsteady gravity current flows over obstacles: Some observations and analysis related to the phase II trials. *Journal of Hazardous Materials* **11**, 325 – 340.

Stone, H. L. 1968 Iterative solution of implicit approximations of multidimensional partial differential equations. *SIAM Journal on Numerical Analysis* **5** (3), 530–558.

Stull, R. 1988 *An Introduction To Boundary Layer Meteorology*. Springer-Verlag New York.

Sumner, J. & Masson, C. 2009 Improving the k-ε turbulence model for simulation of atmospheric boundary layer flow. Openfoam workshop 4.

Tennekes, H. & Lumley, J. L. 1972 *A first course in turbulence*. MIT Press, Cambridge, MA.

Van Ulden, A. P. & Holtslag, A. A. M. 1985 Estimation of atmospheric boundary layer parameters for diffusion applications. *Journal of Climate and Applied Meteorology* **24** (11), 1196–1207.

Vembe, B., Rian, K., Holen, J., Lilleheie, N., Grimsmo, B. & Myhrvold, T. 2010 *Kameleon FireEx 2000 Theory Manual*. Computational Industrial Technologies AS.

Versteeg, H. & Malalasekera 2007 *An Introduction to Computational Fluid Dynamics*, 2nd edn. Pearson Education Limited.

Webber, D., Jones, S. & Martin, D. 1993 A model of the motion of a heavy gas cloud released on a uniform slope. *Journal of Hazardous Materials* **33**, 101 – 122.

White, F. 2006 *Fluid Mechanics*, 6th edn. McGraw-Hill Science/Engineering/-Math.

A Consistent model constants

This appendix presents a derivation of the relation for model constants that are consistent with Monin-Obukhov similarity theory.

The profile equations for the velocity, mean turbulence energy and its dissipation rate are expressed

$$u = u_* \frac{1}{\kappa} \left[\ln(z/z_0) - \psi_M(z/L) + \psi_M(z_0/L) \right], \tag{A.1}$$

$$k = \frac{u_*^2}{\sqrt{C_{\mu 1}}} \left(1 - \frac{z}{h}\right)^2 \tag{A.2}$$

and

$$\varepsilon = \frac{u_*^3}{\kappa} \left(\frac{1}{z} + \frac{4}{L} \right). \tag{A.3}$$

These can be simplified by assuming that the atmospheric stability is neutral (i.e. $L \to \infty$), meaning that the boundary layer height grows indefinitely, $h \gg 1$. Resulting in a constant $k = u_*^2/\sqrt{C_{\mu 1}}$, $\varepsilon = (u_*^3/\kappa)(1/z)$ and a z-derivative of the velocity, by using $\psi_M = -17(1 - e^{-0.29z/L})$, that can be expressed

$$\frac{du}{dz} = \frac{u_*}{\kappa} \left[\frac{1}{z} + \frac{4.93}{L} e^{-0.29z/L} \right], \tag{A.4}$$

which for a neutral atmosphere reduces to

$$\left. \frac{du}{dz} \right|_{L \to \infty} = \frac{u_*}{\kappa} \frac{1}{z}. \tag{A.5}$$

Using k and ε to express ν_t, through $\nu_t = C_\mu k^2/\varepsilon$, gives $\nu_t = u_* \kappa z$.

For a neutral atmosphere, where the buoyancy neither creates nor destroys turbulence, the transport equations for k and ε, by using no low-Reynolds number effects, are

$$\frac{\partial \bar{\rho} k}{\partial t} + \frac{\partial (\bar{\rho} \tilde{u}_i k)}{\partial x_i} = \frac{\partial}{\partial x_i} \left(\frac{\mu_{\text{eff}}}{\sigma_k} \frac{\partial k}{\partial x_i} \right) + \bar{\rho} P - \bar{\rho} \varepsilon \tag{A.6}$$

and

$$\frac{\partial \bar{\rho} \varepsilon}{\partial t} + \frac{\partial (\bar{\rho} \tilde{u}_i \varepsilon)}{\partial x_i} = \frac{\partial}{\partial x_i} \left(\frac{\mu_{\text{eff}}}{\sigma_\varepsilon} \frac{\partial \varepsilon}{\partial x_i} \right) + C_1 \bar{\rho} P \frac{\varepsilon}{k} - C_2 \bar{\rho} \frac{\varepsilon^2}{k}. \tag{A.7}$$

Assuming that any diffusive transport of either quantity is in the vertical direction

only, no lateral gradients and that the solutions are steady, Eq. (A.6) can be reduced to

$$0 = P - \varepsilon, \tag{A.8}$$

which is to say that there is a local equilibrium between production and dissipation rate of k. This can be controlled by using that

$$P = \nu_t \left(\frac{du}{dz}\right)^2 = u_* \kappa z \left(\frac{u_*}{\kappa z}\right)^2 = \frac{u_*^3}{\kappa z} = \varepsilon. \tag{A.9}$$

Note that this would not be the case if there was still a z-dependency in k, which would introduce a diffusive transport of k as well. Neglecting the molecular transport of ε then gives

$$0 = \frac{d}{dz}\left(\frac{u_* \kappa z}{\sigma_\varepsilon}\frac{d\varepsilon}{dz}\right) + (C_1 - C_2)\frac{\varepsilon^2}{k}. \tag{A.10}$$

Inserting for k and ε results in

$$0 = \frac{d}{dz}\left(\frac{u_* \kappa z}{\sigma_\varepsilon}\left(-\frac{u_*^3}{\kappa z^2}\right)\right) + (C_1 - C_2)\sqrt{C_\mu}\frac{u_*^4}{\kappa^2 z^2}, \tag{A.11}$$

which can further be expressed

$$\frac{\kappa^2}{\sigma_\varepsilon} + (C_1 - C_2)\sqrt{C_\mu} = 0, \tag{A.12}$$

where it is important to note that both removed quantities, u_* and z, are positive and greater than zero. Using the standard values, $\sigma_\varepsilon = 1.3$, $C_\mu = 0.09$, $C_1 = 1.44$, $C_2 = 1.92$ and $\kappa = 0.41$ does not fulfill the equation. Freedman & Jacobson (2003) argue that to get a Monin-Obukhov consistent set of constants, σ_ε should be set to 1.1 in the neutral case. This is strictly for a neutral atmosphere, though, which is an undesirable approach to get a diverse solution.

A similar procedure can be done to find consistent values for a stably stratified atmosphere as well. This involves including the turbulence production due to buoyancy, the G term in Eq. (4.43), a term that is now tuned to buoyancy effects related to significant density gradients, and therefore not in effect for an atmospheric flow.